2-14-2014

Facile Synthesis of High Surface Area Molybdenum Carbide and Nitride: An Application in Support Materials for Oxygen Reduction Reaction

Aaron Roy

Aaron Roy
Candidate

Chemical Engineering
Department

This thesis is approved, and it is acceptable in quality and form for publication:

Approved by the Thesis Committee:

Tim L. Ward ,Chairperson

Plamen Atanassov

Alexey Serov

Facile Synthesis of High Surface Area Molybdenum Carbide and Nitride: An Application in Support Materials for Oxygen Reduction Catalysts

by

AARON ROY

B.S. CHEMICAL ENGINEERING, UNIVERSITY OF NEW MEXICO, 2011

THESIS

Submitted in Partial Fulfillment of the
Requirements for the Degree of

Master of Science
Chemical Engineering

The University of New Mexico
Albuquerque, New Mexico

December, 2013

Acknowledgments

My sincere gratitude is extended to Professor Plamen Atanassov and Professor Tim L. Ward for their continual support of my education, for sharing with me their experience, and most importantly for offering to me their guidance through which I have gained invaluable skills which will undoubtedly benefit me both now and in the future.

I also thank my colleagues of whom contributed to this project their own creativity and intellectualism: Alexey Serov, PhD., Kateryna Artyushkova PhD., Angelica Benavidez, Ulises Martinez, PhD., Mayat Smolnik, Lior Elbaz, PhD., and Eric Brosha, PhD.

Facile Synthesis of High Surface Area Molybdenum Carbide and Nitride: An Application in Support Materials for Oxygen Reduction Catalysts

by

Aaron Roy

B.S., Chemical Engineering, University of New Mexico, 2011.
M.S., Chemical Engineering, University of New Mexico, 2013.

Abstract

A method to synthesize high surface area α-$MoC_{(1-x)}$ without the temperature programmed reduction (TPR) of MoO_3 is described. This method was then used, in conjunction with a novel *in situ* method to obtain highly dispersed $PtMo_z$ supported on α-$MoC_{(1-x)}$, to explore the suitability of such materials as catalysts for oxygen reduction reaction (ORR) in a proton exchange membrane fuel cell (PEMFC). $Mg_2(Mo_3O_8)$ and $Zn_2(Mo_3O_8)$, alternative tetravalent Mo intermediates to MoO_2, were obtained through the thermal decomposition of $Mg(MoO_4)$ and $Zn(MoO_4)$ in mixtures of CO and H_2. A novel sacrificial support method was developed where MgO and ZnO were investigated sacrificial support materials formed *in situ* as decomposition products of the Mo precursor. Reaction conditions were explored: including feed composition, synthesis temperature, and synthesis duration. X-Ray powder diffraction (XRD) was used to determine the time dependence on conversion, where 30 to 140 minutes at a temperature of ~700 °C was required to reach full conversion of the precursors. Scanning electron microscopy (SEM) revealed an equiaxed microstructure with primary particle

sizes between approximately 15-30 nm, depending on the duration of high temperature exposure. Rapid heating rates along with limited exposure to high temperature required by this method resulted in gravimetric surface areas as high 45 m^2/g, measured using four point Brunauer-Emmett-Teller (BET) analysis. A similar, ammonia-free, synthesis of β-$MoN_{(1-x)}$ in mixtures of N_2 and H_2 is also described.

The ability of these precursors to be decomposed rapidly, in comparison to the time requirements for TPR, was utilized in the development of an *in situ* method for the preparation of $PtMo_z$ composite phases supported on α-$MoC_{(1-x)}$. Ammonium magnesium molybdate, $(NH_4)_2Mg(MoO_4)_2$, was developed as a precursor to α-$MoC_{(1-x)}$ which was found to form favorable interactions with ammonium derived $(PtCl_6)^{+2}$ species when co-precipitated in $NH_4(OH)$. When this co-precipitated, and amorphous, precursor was treated under the carbiding conditions developed for the synthesis of α-$MoC_{(1-x)}$, highly dispersed $PtMo_z$ on α-$MoC_{(1-x)}$ was obtained. Crystalline platinum phases were not observed by XRD and Transmission Electron Microscopy (TEM) revealed platinum phases with crystalline domains on the order of approximately 5 nm, homogeneously dispersed throughout the observed samples. The materials, as prepared, were found to be catalytically inert for ORR, leading to the development of an additional treatment designed to redistribute platinum phases in a manor conducive for yielding more labile surface species. In particular, it was found that a thermal treatment in a pure CO atmosphere directly following the initial material synthesis resulted in significant development of electrochemical surface area (ECSA). Materials were characterized using cyclic voltammetry (CV) in a rotating disc electrode setup. CV measurements were performed in both O_2 and N_2 saturated solutions of 0.1 M $HClO_4$. The ECSA of this material was measured at ~36 m^2/g and the specific mass activity for ORR was measured to be ~ 137 A/g_{pt}. Catalyst durability measurements were also

performed and the results are reported. The gravimetric surface area of the α-$MoC_{(1-x)}$ support was measured using BET N_2 adsorption, measuring ~32 m^2/g. The catalysts microstructure was also characterized using SEM. Transmission electron microscopy (TEM) was employed for the identification of various possible composite phases ranging from : α-Pt, α-$PtMo_z$, β-Pt_3Mo, and, α-$(Pt2Mo_3C)_{0.66}$. TEM results indicate a more broad distribution of these platinum phases, with the addition of what is likely β-$MoC_{(1-x)}$, in the materials following the CO surface treatment. X-ray photoelectron spectroscopy (XPS) was also used for surface analysis and the results are discussed.

Table of Contents

List of Figures

Introduction

Beginning in the latter part of the 20th century, hydrogen fuel cell technology has received much attention as a promising avenue for providing unconventional forms of energy in a variety of applications, most notably the automotive industry. However, high costs associated with fuel cell catalysts, as well as the durability of these materials, have proven to be a substantial economic constraint. Of particular interest is the low durability of state-of-the-art Pt/C_{black} catalysts due to electrochemical oxidation, and subsequent corrosion, of the carbon support. Specifically, cathode materials supported on carbon are exceptionally vulnerable to corrosion due to electrochemical oxidation of carbon in the presence of water to form CO_2 ($E°=0.207$ V vs. SHE) [1]. The loss of the support results in the detachment of Pt particles which can then, through the process of Ostwald Ripening, agglomerate on the surface which effectively decreases the electrochemical surface area (ECSA) of the catalyst. Pt nano-particles may also be soluble in acidic electrolytes at cell potentials near the upper operating range of a PEMFC [2]. Other phenomena, such as the migration and subsequent sintering of high energy Pt surface particles, also contribute to the loss of ECSA. Another mode of corrosion at the cathode is due to the heterogeneous water gas reaction. Here, Pt can catalyze the oxidation of carbon to form CO and H_2 stoichiometrically, again resulting in a loss of ECSA. As such, it has been proposed to replace carbon with high surface area materials such as transition metal carbides and nitrides which possess high electrical conductivity and corrosion resistant properties under the range of PEMFC operating conditions [3]. Of particular interest is α-$MoC_{(1-x)}$, which has been shown to have a large region of

stability under an applied potential at low pH [4].

Contemporary methods of preparing high surface area α-$MoC_{(1-x)}$ and $MoN_{(1-x)}$ typically require extensive temperature programmed reduction reaction designed to control particle morphology. This, when coupled with the oxophilicity of α-$MoC_{(1-x)}$, create specific engineering challenges involving the dispersion of catalyst phases on the surface of these materials. Therefore, it has been the objective of this work to develop methods of preparing both, high surface area α-$MoC_{(1-x)}$, as well as methods of dispersing active Pt phases on α-$MoC_{(1-x)}$, in ways which address the specific technical challenges associated with the preparation of this specific class of materials. This work describes the methods developed for a more facile preparation of these materials as well as an assessment, via electrochemical characterization, of the suitability of these materials in the application for catalysis of oxygen reduction reaction in a proton exchange membrane fuel cell (PEMFC).

Chapter 1

Synthesis of High Surface area α-$MoC_{(1-x)}$ and β-$MoN_{(1-x)}$

1.1 Introduction

High surface area ceramic materials, such as Mo_2N and Mo_2C, have been investigated for their useful material properties which include, but are not limited to: catalysts for methane reforming, ammonia synthesis, alcohol synthesis from syngas, hydrodesulfurization, and electrocatalysis for hydrogen evolution reaction [5-10]. Additionally, Mo_2C and Mo_2N are known to possess high electrical conductivity, which in combination with their notable material hardness provide the potential to function as corrosion-resistant supports for platinum in PEM fuel cells [3].

Synthesis methods of high surface area Mo_2N and Mo_2C have been reported using a variety of methods, which can be summarized by three main reaction categories: carbothermal reduction, carburization, and ammonolysis of MoO_3 [11-17]. In all three cases the molybdenum precursors are typically MoO_3, $(NH_4)_6Mo_7O_{24}\cdot 4H_2O$ (AHM), or $(NH_4)_2MoO_4$ (AM), where molybdenum is initially hexavalent. During the reduction of the precursor, an intermediate tetravalent phase (MoO_2) is formed which is the species directly converted to nitride or carbide. High rates of solid state diffusion of the intermediate oxide phase, along with slow reduction kinetics, often result in extensive grain growth and low surface area carbides and nitrides [18]. To avoid this, these methods routinely employ temperature programmed reduction reaction (TPR) as a means of minimizing grain growth and maximizing surface area. Although effective,

TPR typically requires long synthesis times at elevated temperature due to slow ramp rates involved in the TPR profile. As a result, TPR may be cost prohibitive to the scaling of these methods and alternative reaction pathways which yield high surface area materials are of interest.

This work focuses on the deliberate selection of molybdenum precursors which decompose in reductive atmospheres resulting in nanocrystalline Mo_2C or Mo_2N, selectively and without the formation of intermediate MoO_2. However, considerable attention has been placed on the synthesis of the cubic phase of Mo_2C, α-$MoC_{(1-x)}$.

The approach has been to achieve rapid conversion of the Mo precursor by arresting certain tetravalent molybdate intermediates, using high temperature along with rapid ramp rates to maximize rates of formation of desired phases while minimizing sintering processes. A sacrificial support method has also been adopted in which a sacrificial material is used to minimize contact between grain boundaries, thus preventing sintering and agglomeration of both molybdate intermediates as well as the carbide/nitride reaction products. In a slight variation of the sacrificial support method (SSM) commonly reported [19-24], reported here is a novel approach in which the sacrificial material is formed *in situ* as a decomposition product of the molybdenum precursor.

1.2 Experimental

1.2.1 Preparation of $Mg(MoO_4)$ and $Zn(MoO_4)$

Molybdic acid, $H_2(MoO_4)$, was prepared by adding MoO_3 powder (Sigma-Aldrich) to an excess amount of 30 wt% H_2O_2 (Sigma-Aldrich).The mixture was heated on a hot plate until the MoO_3 was fully dissolved and the solution, yellow in color, became transparent. The solution of $H_2(MoO_4)$ and excess H_2O_2 was brought to a boil to decompose excess peroxide. Next, the $H_2(MoO_4)$ was removed from the hot plate and an excess amount of MgO powder (UBE Material Industries, Ltd.) was added directly to $H_2(MoO_4)$. The resulting acid/base reaction produces magnesium molybdate, $Mg(MoO_4)$. Water soluble $Mg(MoO_4)$ was then isolated by the filtration of insoluble MgO, which was added in excess to insure complete conversion of $H_2(MoO_4)$. The solution of $Mg(MoO_4)$ was then brought to a boil on a hot plate until dried and the crystalized $Mg(MoO_4)$ was collected.

For the preparation of $Zn(MoO_4)$, the procedure for $Mg(MoO_4)$ synthesis was modified slightly. As $Zn(MoO_4)$ is insoluble in water, high purity ZnO (Sigma-Aldrich) was added to an excess amount of $H_2(MoO_4)$. The precipitate, $Zn(MoO_4)$, was then isolated by centrifuging the reaction mixture, decanting the excess $H_2(MoO_4)$, and then adding deionized water. This step was repeated until all excess $H_2(MoO_4)$ was removed. The $Zn(MoO_4)$ precipitate was then placed in an oven and dried in air at ~100 °C for several hours. It is important to note that this procedure yields a monoclinic phase of $Zn(MoO_4)$, where a triclinic phase can be prepared by slight modification of this procedure. In the case of $Zn(MoO_4)$ and $Mg(MoO_4)$ the monoclinic structures were used explicitly in this study.

1.2.2 Synthesis of α-$MoC_{(1-x)}$ in Syngas

For the preparation of α-$MoC_{(1-x)}$, 0.4 g of $Mg(MoO_4)$ or $Zn(MoO_4)$ was placed in a 7 mL porcelain combustion boats inside of a 1 inch diameter quartz tube. The quartz tube was then heated using a 14 inch single zone tube furnace in a 1:4 molar mixture of CO-H_2 at a total volumetric flow rate of 200 mL/min. The reactor temperature was ramped from ambient temperature to 700 °C at a rate of ~40 °C/min.

In the case of $Mg(MoO_4)$, the synthesis temperature of 700 °C was held for 2.0 hours under continuous flow of a 1:4 molar mixture of CO-H_2 at a rate of 200 mL/min, followed by a treatment in pure H_2 at a flow rate of 120 mL/min at 700 °C for 20 minutes. For the synthesis of α-$MoC_{(1-x)}$ using $Zn(MoO_4)$, the synthesis temperature of 700 °C in a 1:4 molar mixture of CO-H_2 was maintained for only 30 minutes, there was no addition H_2 treatment. After the heat treatment, all samples were cooled to ~400 °C under syngas where the carrier was then switched to a flow of industrial grade argon. The quartz reactor tubes were then removed from the furnace and allowed to cool to ambient temperature under argon flow. Once at ambient temperature, the flow was switched to 2 mol% O_2 with a He balance for ~1 hour. This step is intended to passivate the α-$MoC_{(1-x)}$ surface with oxide to inhibit bulk oxidation of the material upon exposure to atmospheric partial pressures of O_2.

In both cases, the decomposition products, MgO and ZnO respectively, were removed by etching in 7M HCl. The products were then washed in deionized water by centrifuging followed by decanting of soluble phases. This process was repeated until a neutral pH was achieved, approximately 6 wash cycles, and the samples were then dried at ~85 °C in air for 12-18 hrs.

1.2.3 Characterization

Materials morphology, purity, and surface area were characterized using scanning electron microscopy (SEM), powder X-ray diffraction (XRD), and Brunauer–Emmett–Teller N_2 adsorption (BET).

Powder X-ray diffraction analysis was performed using a Rigaku Smartlab with Brag-Brentano focusing and Cu K_α radiation (40 kV, 40 mA). The detector used was the Rigaku D/teX Ultra 250 1D silicon strip detector. Scanning Electron Microscopy was performed using a Hitachi S-5200 SEM where powder samples were disbursed ontocarbon tape adhered to an aluminum sample plate. The accelerating voltage used was 2 kV. Surface areas were measured using N_2 adsorption via four point BET analysis, carried out in a Micrometrics 2360 Gemini Analyzer.

1.3 Results and discussion

1.3.1. Sacrificial Support Method and Non-Oxide Reaction Pathway

The sacrificial support method (SSM) has been extensively used as a generalized method for creating a variety of high surface area materials. In many cases high surface area silica is used as the sacrificial material, which is removed by post processing in either KOH or HF. In the present work, we present a modification to the SSM method where the sacrificial support is formed *in situ* as a decomposition product of the Mo precursor, eliminating lengthy pre-processing methods required by the SSM method. A reaction mechanism was proposed where various sheelite salts with the general formula $M(MoO_4)$ were used as Mo precursors; where M may be any

divalent metal cation (Be, Mg, Ca, Sr, Ba, Mn, Zn). These salts were selected on a basis of two criteria. The first being that the metal, M, must form a stable oxide, thus satisfying the general redox reaction described by Equation (1).

$$M(MoO_4) + R + 3H_2 \longrightarrow MO + 3MoR_{(1-x)} + 3H_2O \quad (1)$$

R = carbon or nitrogen source

Equation (1) is written in a general form intended to balance only those species directly involved in the reduction of molybdenum. R may contain other species, not being C or N, which may be balanced with H_2 in stoichiometric proportions not shown. Also, the variable "x" is bound between 0 and 0.5 for α-MoC as well as between 0.67 and 0.72 for β-MoN; see the phase diagrams for molybdenum carbide and nitride in Appendix-C.

The intended role of the oxide product is to provide resistance to solid-state mass transfer, effectively preventing the coarsening of grain boundaries. The result of which is likely to produce smaller grain sizes, smaller primary particle sizes, and greater specific surface area of molybdenum carbide and nitride.

As previously described, the reaction pathway to molybdenum carbide and nitride commonly proceeds through a tetravalent molybdenum oxide intermediate, MoO_2 [6,16,18]. As it has been suggested that MoO_2 is an undesired intermediate phase to high surface area molybdenum carbide and nitride, a second criterion to the proposed reaction mechanism was established. This criteria states that these $M(MoO_4)$ salts must decompose reductively to form a tetravalent molybdate. This criteria acknowledges the fact that $Mo^{(IV)}$ is the common valency between oxide, carbide, and nitride. Therefore, a tetravalent molybdate is required for the proposed reaction pathway to carbide or nitride

that is not to proceed through MoO_2.

Based on the first criteria, Mg and Zn were selected as the most promising cations to be used in this method due to the stability of MgO and ZnO. To identify possible intermediate species, $Mg(MoO_4)$ was partially decomposed at 500 °C in a 5 mol% flow of NH_3, N_2 balance, for ~30 minutes. The decomposition products of $Mg(MoO_4)$ were compared to that of AHM treated under identical conditions. XRD patterns in Figure-1, for both cases, show the reduction of molybdenum, initially $Mo^{(VI)}$, to a valence state of four.

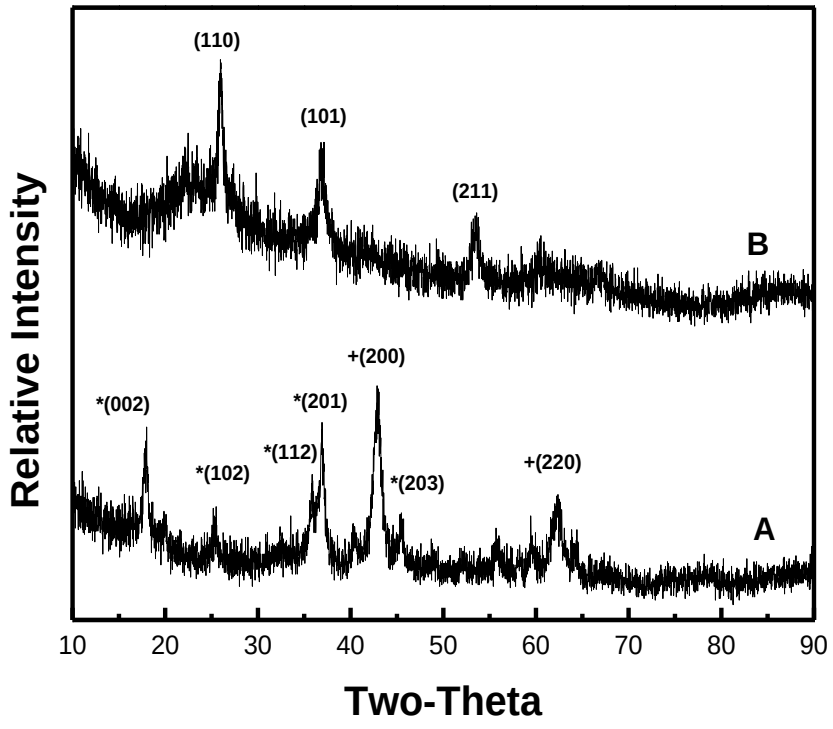

Figure 1.1 XRD patterns of intermediate species from the decomposition of **(A)** $Mg(MoO_4)$ to MgO (+) and $Mg_2(Mo_3O_8)$ (*), and **(B)** AHM to MoO_2 in a 5 mol% flow of NH_3 at 500 °C for ~30 min. *All peak intensities are normalized to the (200) reflection of MgO in (A).*

This result suggests that dimagnesium-trimolybdate, $Mg_2(Mo_3O_8)$, can replace MoO_2 as the intermediate phase to carbide or nitride when starting from $Mg(MoO_4)$. It

was also verified that $Zn(MoO_4)$ decomposes to an analogous $Zn_2(Mo_3O_8)$ and ZnO under identical conditions. Thus, $Mg(MoO_4)$ and $Zn(MoO_4)$ satisfy both criteria, establishing these salts as possible precursors to α-$MoC_{(1-x)}$ and β–$MoN_{(1-x)}$.

From this, an overall two-step reaction pathway was proposed and is described by Equations (2) and (3) for the case of $Mg(MoO_4)$ reacting to α-$MoC_{(1-x)}$ using CO as a carbon source.

$$3Mg(MoO_4) + 3H_2 \longrightarrow MgO + Mg_2(Mo_3O_8) + 3H_2O \quad (2)$$

$$Mg_2(Mo_3O_8) + 3CO + 9H_2 \longrightarrow 2MgO + 3MoC_{(1-x)} + 9H_2O \quad (3)$$

1.3.2 Synthesis of α-$MoC_{(1-x)}$ from $MgMoO_4$

α -$MoC_{(1-x)}$ was prepared by the reaction of $Mg(MoO_4)$ in mixtures of CO and H_2. The molar ratio of CO to H_2 was held constant at 1:4 and synthesis temperatures were varied from the approximated thermodynamic minimum of 469 °C, where $\Delta_rG°=0$, to ~ 25 °C below an upper limit determined experimentally [17]. The upper limit was defined as the onset temperature when the formation of hexagonal phase molybdenum carbide, β-Mo_2C, was observed. The purpose for this was to selectively exclusively produce cubic α-$MoC_{(1-x)}$ at a maximum rate of reaction. The upper temperature limit was found to be ~ 725 °C.

XRD was used to study the effect of synthesis time on conversion. Samples were heat treated at 700 °C from 1.0 - 2.5 hours, followed by passivation in a low concentration of O_2 then post processing in HCl to etch MgO. Whole pattern fitting (WPF) using MDI JADE 2010™ analytical software was used to determine relative

ratios of α-$MoC_{(1-x)}$ and $Mg_2(Mo_3O_8)$. This data was then used to calculate total molar conversion. Conversion was also calculated through a material balance based on experimental and theoretical yield. Material balance calculations were in agreement with XRD WPF calculations within approximately ± 5 %. Figure-1.2 shows XRD patterns for samples heat treated for1.0hr, 1.5hr, 2.0hr, and 2.5hr under identical conditions. Molar conversions of $Mg_2(Mo_3O_8)$ were calculated to be ~ 10, 35, 60, and 65% respectively. Results show the observed rate of reaction (3) slows significantly with increased conversion and that the rate limiting step is the decomposition of $Mg_2(Mo_3O_8)$, not the decomposition of $Mg(MoO_4)$.

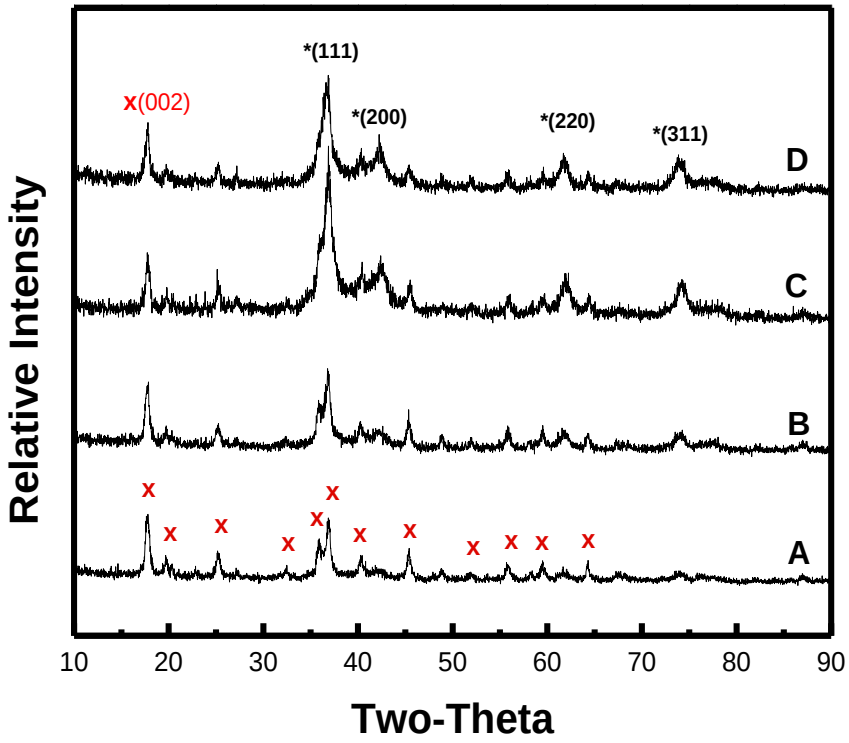

Figure 1. 2 XRD patterns showing conversion of $Mg_2(Mo_3O_8)$ to α-$MoC_{(1-x)}$ at 700°C:**(A)** ~10 % conversion after 1.0 hr, **(B)** ~35 % after 1.5 hr, **(C)**, ~60 % after 2.0 hr, and **(D)** ~65 % after 2.5 hr. In all samples MgO was etched using HCl. *All peaks are normalized to the (002) reflection of $Mg_2(Mo_3O_8)$ in "A", of which reflections are denoted by "x". α - $MoC_{(1-x)}$ reflections denoted by (*).*

An additional reaction where α-$MoC_{(1-x)}$ can be used as a carbon source was investigated. Here, the reduction of $Mg_2(Mo_3O_8)$ by H_2 provides the necessary redox potential for the direct reaction of solid species α-$MoC_{(1-x)}$ and $Mg_2(Mo_3O_8)$.

$$Mg_2(Mo_3O_8) + 3MoC_{1-x} + 6H_2 \longrightarrow 2MgO + 3MoC_{1-y} + 6H_2O \quad ; \quad x < y \tag{4}$$

Reaction (4) allows for a carbon rich phase of α-$MoC_{(1-x)}$ to be converted to a molybdenum rich phase by the removal of the carbon source from the feed. An assumption was made that α-$MoC_{(1-x)}$ produced from Reaction (3) serves as the sole carbon source for reaction (4) and that x=0. These assumptions then set a minimum intermediate molar conversion, based on Reaction (3), of $Mg_2(Mo_3O_8)$ at 50 %, prior to the use of Reaction (4). At intermediate conversions of Reaction (3) less than 50 %, $Mg_2(Mo_3O_8)$ will be reduced to molybdenum as the available carbon is becomes depleted. This corresponds to x=0.5. Once this minimum conversion was reached, the CO feed was stopped and pure H_2 was used to carry out the additional heat treatment, again at 700 °C.

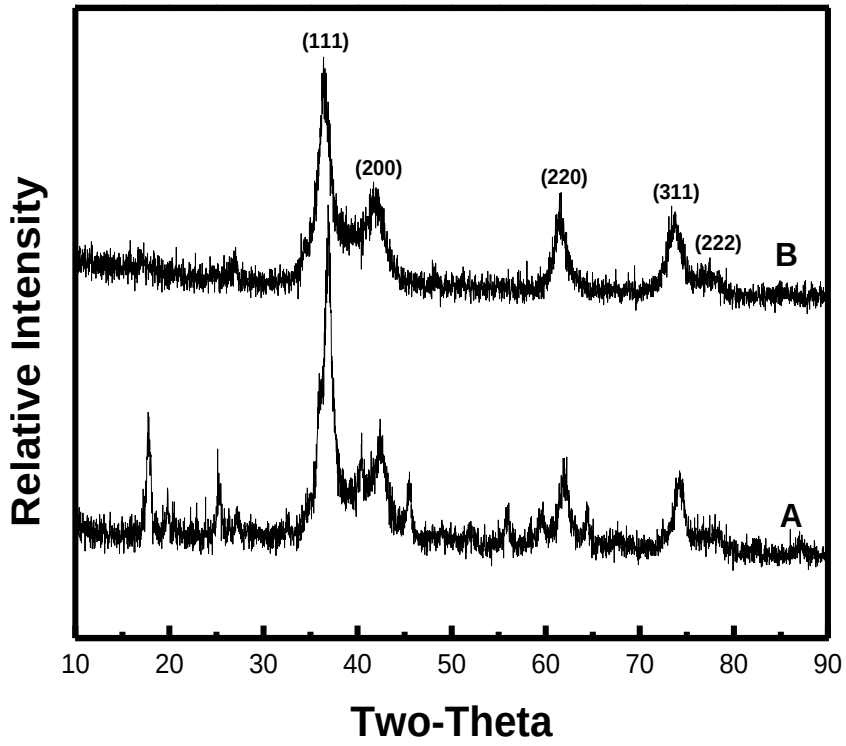

Figure 1. 3 XRD patterns showing conversion of $Mg_2(Mo_3O_8)$ to **(A)** α-$MoC_{(1-x)}$ at 60 % conversion after 2 hr of reaction (2) at 700 °C, and **(B)** α-$MoC_{(1-y)}$ at 95 % conversion after 2 hr of Reaction (2) at 700 °C followed by 10 min of reaction (3). *In both samples, MgO was etched using HCl.*

Figure-1.3 shows the rapid conversion reached, from an intermediate conversion 65 % to 95 % after only 10 minutes in pure H_2. Further evidence of this reaction can be seen by XRD as subtle shifts in the peak positions to slightly lower values of 2θ. This is an expected result for a shift from a carbon rich phase to a Mo rich phase of α-$MoC_{(1-y)}$, indicating a decreasing lattice parameter with decreasing carbon content.

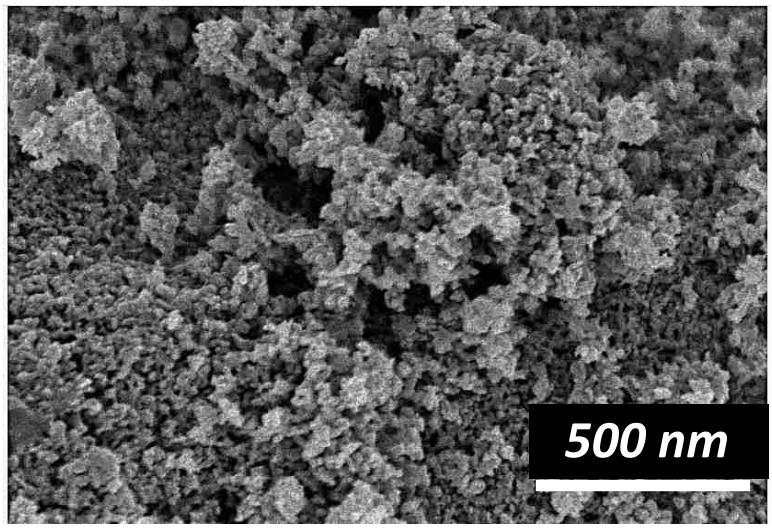

Figure 1.4 SEM image of α-$MoC_{(1-y)}$ prepared using $Mg(MoO_4)$ in a 1:4 molar flow of $CO-H_2$ at 700 °C for 2 hours followed by treatment in pure H_2 for 20 minutes. MgO was etched by HCl.

Additional samples were prepared under the conditions described by Reaction (4) where it was found that a total of 20 minutes were required to obtain complete conversion of $Mg_2(Mo_3O_8)$ to α-$MoC_{(1-y)}$. Sample purity was confirmed by XRD. SEM images in Figure-1.4 show this material to possess a relatively uniform and equiaxed primary particle size between approximately 15 nm and 30 nm, with agglomerates on the order of sever microns. The specific surface area was measured, using four point BET analysis, to be 35 m^2/g. This result is consistent with an average particle size of 20 nm.

1.3.3 Synthesis of α-$MoC_{(1-x)}$ from $Zn(MoO_4)$ in Syngas

$Zn(MoO_4)$ was studied as an alternative precursor to $Mg(MoO_4)$. Initially, $Zn(MoO_4)$ was used in an attempt to eliminate post processing in HCl by making use of the volatile decomposition of ZnO, occurring in a H_2 atmosphere and at temperatures

near 650°C [25]. Analogous to the synthesis of α-$MoC_{(1-x)}$ using $Mg(MoO_4)$, $Zn(MoO_4)$ was found to decompose to an intermediate dizinc-trimolybdate phase, $Zn_2(Mo_3O_8)$. This intermediate was then treated in a 1:4 molar ratio of CO to H_2 at 700 °C where the observed rate of reaction was found to be much greater than in the case of $Mg_2(Mo_3O_8)$. Unlike $Mg_2(Mo_3O_8)$, where conversion to α-$MoC_{(1-x)}$ was less than 10 % after 1.0 hours, $Zn_2(Mo_3O_8)$ was converted entirely to α-$MoC_{(1-x)}$ in as little as 0.5 hours. Figure-1.5A shows the rapid conversion of $Zn_2(Mo_3O_8)$ to α-$MoC_{(1-x)}$ obtained after only 30 minutes at 700 °C.

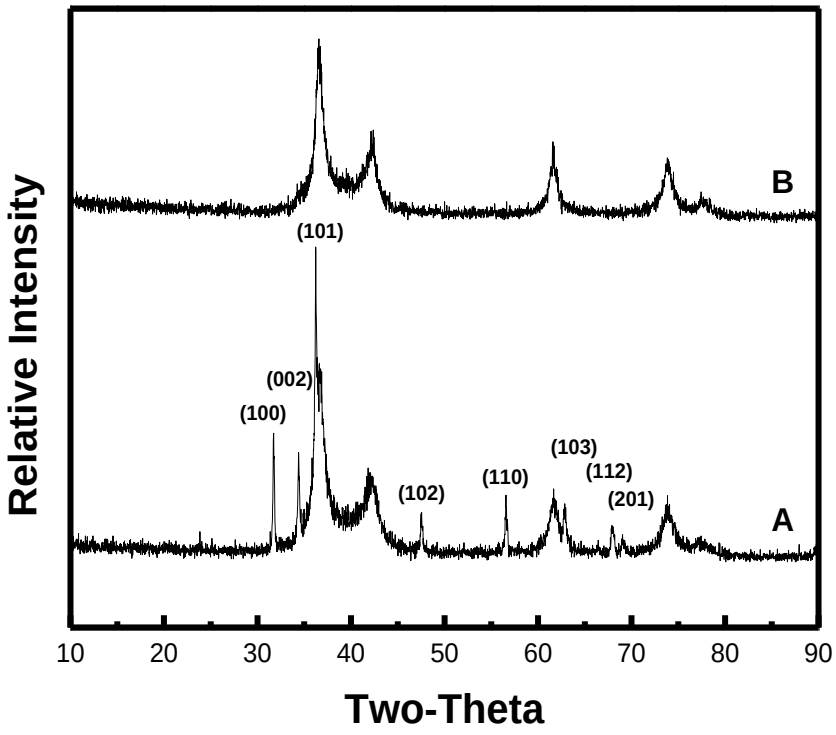

Figure 1.5 XRD patterns showing **(A)** conversion of $Zn_2(Mo_3O_8)$ to α-$MoC_{(1-x)}$ and ZnO at in a 1:4 molar flow of CO-H_2 at 700 °C for 30 minutes, and **(B)** thermal removal of ZnO in a 1:4 molar flow of CO-H_2 at 700 °C for 5 hours.α-*$MoC_{(1-x)}$ reflections are not labeled.*

ZnO was successfully removed by volatilization of Zn produced by the thermal decomposition of ZnO in H_2, Equation (5). This process was carried out under the

synthesis conditions of a 1:4 molar ratio of CO to H_2 at 700 °C. A total of ~5 hours were required to remove ZnO below trace amounts found by XRD, Figure-1.5B. Attempts were made to accelerate the decomposition of ZnO in pure H_2 and at higher temperature; however these attempts resulted in the formation of hexagonal carbide, β-Mo_2C. It is unclear as to what role CO plays in the inhibition of this phase transition.

$$ZnO + MoC_{(1-x)} + H_2 \longrightarrow Zn_{(v)} + MoC_{(1-x)} + H_2O \quad (5)$$

No evidence of $Zn_2(Mo_3O_8)$ was found in either sample prepared with and without the thermal removal of ZnO described by Reaction (5). Although ZnO was successfully removed *in situ*, bulk sintering at these temperatures is a concern and HCl was favored for the etching of ZnO to yield higher surface area materials. SEM images shown in Figure-1.6 reveal a more nanocrystalline morphology of α-$MoC_{(1-x)}$ than was achieved using $Mg(MoO_4)$. Primary particle sizes were found to be approximately < 20 nm which is consistent with the surface area measured by BET, ~45 m^2/g. The significant increase in surface area obtained using $Zn(MoO_4)$ is directly attributed to the rapid rate of reaction, and low overall synthesis time, reducing the effects of sintering and grain coarsening.

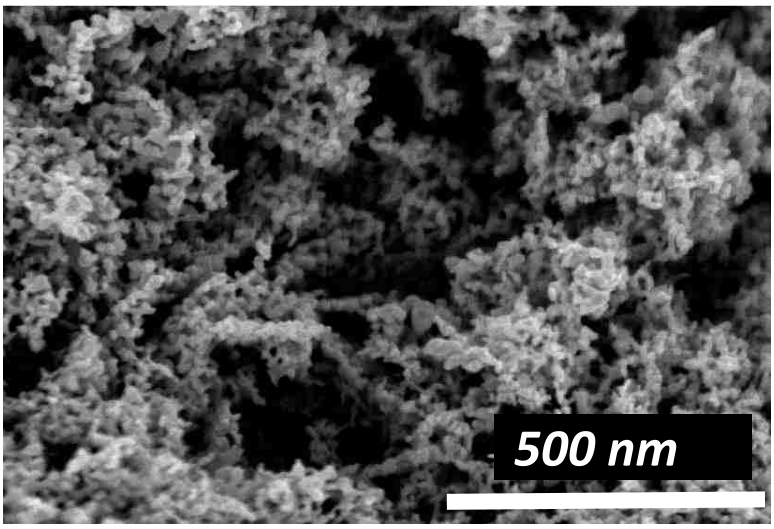

Figure 1.6 SEM image of α-$MoC_{(1-x)}$ prepared by the reaction $Zn(MoO_4)$ in a 1:4 molar flow of CO-H_2 at 700 °C for 30 minutes. ZnO was etched by HCl.

1.3.4 Synthesis of β-$MoN_{(1-x)}$ from $MgMoO_4$ in Forming Gas

The most effective method for synthesizing high surface area molybdenum nitride was developed by Leo Volpe by the temperature programmed reduction of MoO_3 in NH_3 [11]. To address the logistical difficulties associated with this method, it was attempted to eliminate TPR from the synthesis of high surface area β-$MoN_{(1-x)}$ and simultaneously demonstrate the capability to do so using an ammonia-free synthesis. Reaction (1) was again applied using $Mg(MoO_4)$, where R = N_2. An overall pathway to β-$MoN_{(1-x)}$ in a mixture of N_2-H_2 is described by Reactions (6) and (7).

$$3Mg(MoO_4) + 3H_2 \longrightarrow MgO + Mg_2(Mo_3O_8) + 3H_2O \quad (6)$$

$$Mg_2(Mo_3O_8) + N_2 + 6H_2 \longrightarrow 2MgO + 3MoN_{(1-x)} + 6H_2O \quad (7)$$

Initially, the molar ratio of N_2-H_2 was chosen to be 1:4 at a synthesis temperature of 700 °C, modeled after the synthesis of α-$MoC_{(1-x)}$. Under these conditions, it was found that this reactive atmosphere was insufficient for nitride formation of for significant decomposition of $Mg_2(Mo_3O_8)$, where Mo metal was the primary decomposition product observed, shown in Figure-1.7A. Temperatures were gradually increased, using a 1:4 molar ratio of N_2-H_2, until β-$MoN_{(1-x)}$ was observed as a reaction product. At 900 °C $Mg_2(Mo_3O_8)$ was seen to form β-$MoN_{(1-x)}$ as a minor product with Mo metal being the dominant product, Figure-1.7B.

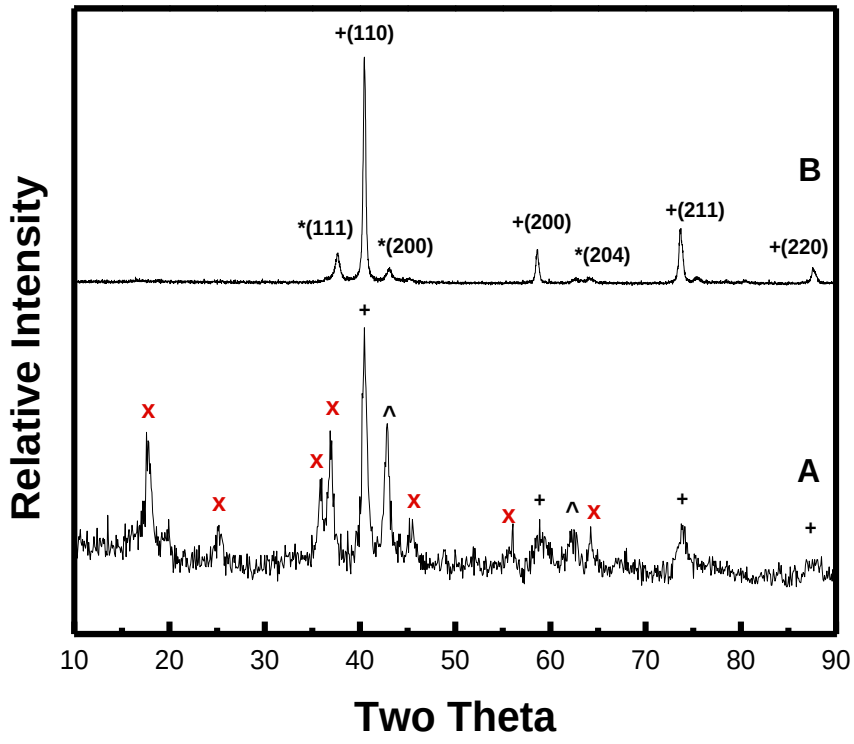

Figure 1.7 XRD patterns showing **(A)** conversion of $Mg_2(Mo_3O_8)$ to Mo metal in a 1:4 molar flow of N_2-H_2 at 700 °C for 30 minutes, and **(B)** conversion of $Mg_2(Mo_3O_8)$ to β-$MoN_{(1-x)}$ and Mo metal under identical flow conditions at 900 °C for 1 hour, MgO was etched by HCl in the sample shown in (B). *All peaks are normalized to the Mo (110) reflection in (A). Reflections of specific phases are denoted as follows: $Mg_2(Mo_3O_8)$ "x", MgO "^", Mo "+", and β-$MoN_{(1-x)}$ "*".*

Next, the concentration of N_2 was gradually increased, at a temperature of 900 °C, until the hexagonal phase, β-$MoN_{(1-x)}$, was produced without evidence of Mo metal. This occurred when the molar ratio of N_2-H_2 used was 7:3 and at a temperature of 900 °C for 2 hours, shown in Figure-1.8. After etching MgO in HCl, BET surface area was measured to be ~12 m^2/g, where SEM images (inset on Figure-1.8) show primary particle sizes on the order of ~50-100 nm. Lower temperatures were explored in attempts to increase surface area by reducing the effects of sintering, however slow rates of conversion and lengthy synthesis durations resulted in the production of metallic Mo. Further experimentation is needed to establish whether the use of $Zn(MoO_4)$ as a nitride precursor will allow for lower temperature, shorter synthesis, and the production of higher surface area nitride phases.

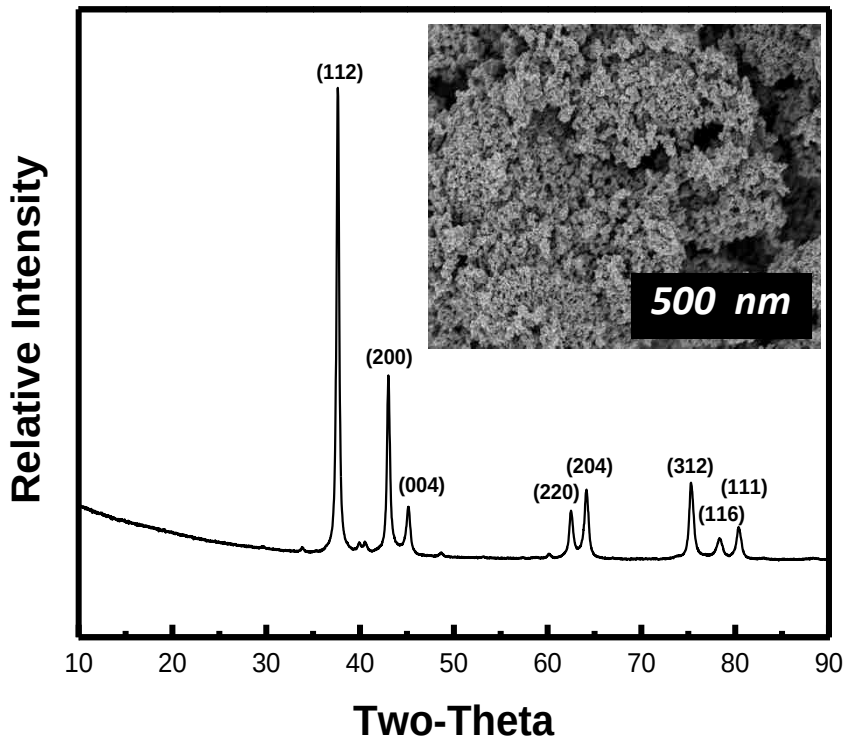

Figure 1.8 XRD patterns showing conversion of $Mg_2Mo_3O_8$ to Hexagonal β-$MoN_{(1-x)}$ in a 7:3 molar flow of N_2-H_2 at 900 °C for 2 hours. Sample was washed in HCl to remove MgO. Inset shows SEM image of β-$MoN_{(1-x)}$

1.4 Conclusion

High surface area α-$MoC_{(1-x)}$ was synthesized in mixtures of CO and H_2 at 700 °C without the aid of temperature programmed reduction. $Mg(MoO_4)$ and $Zn(MoO_4)$ were used as Mo precursors where the resulting α-$MoC_{(1-x)}$ possessed surface areas, measured by BET analysis, of 35 m^2/g and 45 m^2/g respectively. MoO_2 was successfully replaced as a reaction intermediate by the tetravalent molybdenum compounds $Mg_2(Mo_3O_8)$ and $Zn_2(Mo_3O_8)$, which form MgO and ZnO as partial decomposition products. An equiaxed and porous morphology was observed in the α-$MoC_{(1-x)}$ samples prepared using this method, with primary particle sizes typically ranging from

15-30 nm. Reaction conditions were explored: including feed composition, synthesis temperature, and synthesis duration, in efforts to maximize the rate of conversion to α-$MoC_{(1-x)}$. A high surface area hexagonal phase of β-$MoN_{(1-x)}$ was also produced without TPR using $Mg(MoO_4)$, although a much higher temperature was required for this synthesis (900 °C). This high temperature, compared to the carbide synthesis temperature of 700 °C, resulted in significantly less surface area in the β-$MoN_{(1-x)}$ samples, ~12 m^2/g. The key result in the synthesis of β-$MoN_{(1-x)}$ was the use of N_2-H_2 mixtures as the reactive atmosphere. This demonstrates that high surface area molybdenum nitride phases can be prepared without TPR, and perhaps more useful, without using NH_3 as a nitrogen source.

Chapter 2

Oxygen Reduction on α-$MoC_{(1-x)}$ Supported $PtMo_z$

2.1 Introduction

Platinum and platinum composite materials have been extensively used in the field of catalysis due to the various inherent catalytic properties of platinum [24, 26-31]. More specifically, proton exchange membrane fuel cells (PEMFC's) have exploited platinum as a catalyst for oxygen reduction reaction (ORR); a four-electron transfer reaction which platinum is able to catalyze in a single step. Efficient kinetics and a low overpotential for ORR make platinum the state-of-the-art catalyst for ORR, thus setting the performance benchmark for ORR catalyst design [32-37]. The cost of platinum, and significant performance degradation due to the electrochemical corrosion of traditional support materials, specifically carbon, gives rise to the basis of several design considerations necessary for the efficient use of platinum as an ORR catalyst. Considerations such as increasing the durability of platinum catalysts by the proposed use of durable support materials such as transition metal nitride or carbide based ceramics. Another important consideration is to maximize the mass activity of platinum. This can be accomplished by achieving highly dispersed platinum particles on the surface of the support, thus maximizing the surface to volume ratio of platinum.

In the present work, cubic phase α-$MoC_{(1-x)}$ was used as a support due to its high electrical conductivity as well as the large region of stability of α-$MoC_{(1-x)}$ in acidic media predicted by previous studies [38]. However, passivation oxide on the surface of α-$MoC_{(1-x)}$ complicates traditional chemical and thermal reduction methods commonly

employed for platinum dispersion. To overcome such difficulties an *in stu* method of platinum dispersion was pursued. This approach regards the catalyst, a $PtMo_z$ composite, and catalyst support as a single multi-component system, where certain components of the catalyst species are derived directly from the support itself. In chapter 1, high surface area molybdenum carbide and nitride ceramics were prepared using a novel method which does not rely on temperature programmed reduction as the mode of achieving surface area, rather on the use $Mg(MoO_4)$ and $Zn(MoO_4)$ which decompose reductively in a manor found to favor the formation of high surface area products. Here, this method has been modified by using $(NH_4)_2Mg(MoO_4)_2$, which further reduces the time duration, as well as temperature requirement, to obtain full conversion of the ceramic precursor. This modification, in combination with a chemical method of obtaining desirable interactions between platinum and molybdenum precursors, allows for an *in situ* method of creating a highly dispersed $PtMo_z$ composite catalyst supported on α-$MoC_{(1-x)}$. This method has, with platinum loadings as low as 7.5 wt%, resulted in catalysts with an electrochemical surface area of ~36 m^2/g and a platinum mass activity of 137 A/g_{Pt} ,comparable to that of commercially available platinum supported on carbon black [39, 40]. Although these catalysts do not possess the desired improvement in durability for ORR, this work demonstrates the capability of producing highly dispersed, platinum or platinum composite catalysts, using a simple *in situ* synthesis.

2.2 Experimental

2.2.1 Synthesis of $PtMo_z$ supported on α-$MoC_{(1-x)}$

The molybdenum precursor, $(NH_4)_2Mg(MoO_4)_2$, was prepared by a slight modification of a method described in Chapter 1 for preparing $Mg(MoO_4)$. Upon the formation of molybdic acid, $H_2(MoO_4)$, MgO (UBE Material Industries, Ltd) was added in a 2:1 molar ratio of Mo to Mg. Next, an excess of saturated $NH_4(OH)$ solution was added during continuous heating on a hot plate. Once the reaction appeared to reach completion the product was dried in air at 85 °C. Next, a known amount of $(NH_4)_2Mg(MoO_4)_2$ was dissolved in deionized water and brought to a boil. An appropriate amount of $H_2(PtCl_6)$ was dissolved in deionized water then added to the boiling solution of $(NH_4)_2Mg(MoO_4)_2$; the amount of $H_2(PtCl_6)$ added was based on a desired mass loading of Pt on α-$MoC_{(1-x)}$. An excess of saturated $(NH_4)OH$ solution was then added to the boiling mixture where continuous heat was applied until a white precipitate was formed. The precipitate was allowed to dry completely in air at 85°C. Once dried the precursor was finely ground using a mortar and pestle.

Approximately 0.5 g of the ground precursor was then placed in a 7 mL porcelain combustion boat then placed inside of a 1 inch diameter quartz tube. The quartz tube was then heated using a 14 inch single zone tube furnace. A 1:4 molar mixture of CO-H_2 at a total volumetric flow rate of 200 mL/min was used as the reaction atmosphere. The reactor temperature was ramped from ambient temperature to 675 °C at a rate of ~40 °C/min. After 1.5 hours at 675 °C, the reactor was cooled to 650 °C and the feed was switched to a pure CO atmosphere at a rate of 100 mL/min. After 2 hours, the reactor was cooled to room temperature, the feed was

switched to 2 % O_2 with a He balance, and these conditions were maintained for ~12-18 hours in order to passivate the α-$MoC_{(1-x)}$ catalyst surface. The powder was then removed from the furnace and was etched in 7 M HCl to remove MgO. The product was then washed in deionized water by identical procedures described in section 1.2.1. Samples were then washed, 2 additional cycles, in 200 proof ethanol then dried in vacuum (~ 30 inHg) at room temperature for ~12-18 hours.

2.2.2 Catalyst Characterization

As described in chapter 1.2.3, the catalysts were characterized using powder X-ray diffraction analysis, SEM imaging, and BET surface area measurements. Additional characterization was performed using X-ray photoelectron spectroscopy for surface composition analysis (XPS), transmission electron microscopy (TEM), and electrochemical measurements conducted in a three electrode half-cell using cyclic voltammetry.

Surface analyses of the catalysts by X-ray photoelectron spectroscopy (XPS) utilized a Kratos Analytical AXIS Ultra DLD Imaging System with an Al K-alpha X-ray source operating at 225 W. High-resolution C 1s, O 1s, Mo 3d and Pt 4f spectra were acquired at 20 eV pass energy for 2, 2, 5 and 10 min respectively. Data analysis and quantification were performed using Casa XPS software.

Electrochemical measurements of ORR performance were conducted in a three electrode cell with 0.1M $HClO_4$ as the electrolyte. A rotating disk electrode (RDE) was used as the working electrode and a real hydrogen electrode (RHE) as the reference electrode. Forming gas, consisting of 6% H_2, was used at the reference electrode for

which a correction of +39 mV to all experimentally collected data was applied. A Pine Instrument Company rotator was used to collect ORR data at 100, 225, 400, 625, and 900 RPM at a scan rate of 5 mV/s and 100 mV/s in both O_2 and N_2 saturated electrolyte.

TEM images were acquired using a JEOL 2010 instrument with an accelerating voltage of 200kV. Data analysis was performed using GATAN Digital Micrograph software where TEM images were digitally converted into spot diffraction patterns using the built in script files "diffractogram3.s". These diffraction patterns were then used to measure crystallite d-spacing values by utilizing the built in script file "peak4.s".

2.3 Results and Discussion

2.3.1 Synthesis of α-$MoC_{(1-x)}$ from $(NH_4)_2Mg(MoO_4)_2$ in Syngas

As described in Chapter 1, $Mg(MoO_4)$ and $Zn(MoO_4)$ have been shown to be useful precursors in the synthesis of α-$MoC_{(1-x)}$ and β-$MoN_{(1-x)}$ phases in mixtures of CO-H_2 and N_2-H_2 respectively. The primary advantage being the ability of these precursors to decompose to high surface area (30-45 m^2/g) α-$MoC_{(1-x)}$ without the necessity of TPR as the primary means of producing surface area. Here, the co-crystallized product of $Mg(MoO_4)$ and $(NH_4)_2(MoO_4)$, $(NH_4)_2Mg(MoO_4)_2$, has been found to decompose to α-$MoC_{(1-x)}$ and β-$MoN_{(1-x)}$ phases more rapidly than $Mg(MoO_4)$, described by the following redox reactions:

$$(NH_4)_2Mg(MoO_4)_2 + CO + 8H_2 \longrightarrow MgO + 2MoC_{(1-x)} + 8H_2O \quad (8)$$

$$(NH_4)_2Mg(MoO_4)_2 + N_2 + 7H_2 \longrightarrow MgO + 2MoN_{(1-x)} + 7H_2O \quad (9)$$

Equations (8) and (9) are written in a form intended to balance only those species directly involved in the reduction of molybdenum. The N species on the reactant side may be balanced with H_2 in stoichiometric proportions not shown.

XRD patterns in Figure-2.1 show the reaction products described by Reactions (8) and (9). The rate of α-$MoC_{(1-x)}$ production was found to be approximately twice that which was observed when pure $Mg(MoO_4)$ was used, while at a temperature lower by 25 °C. This rapid rate of α-$MoC_{(1-x)}$ production is considered an integral factor in the *in situ* platinum dispersion method described in section 2.3.2. More notably, β-Mo_2N was prepared at 750 °C, a temperature 150 °C lower than the minimum nitriding temperature attainable using pure $Mg(MoO_4)$.

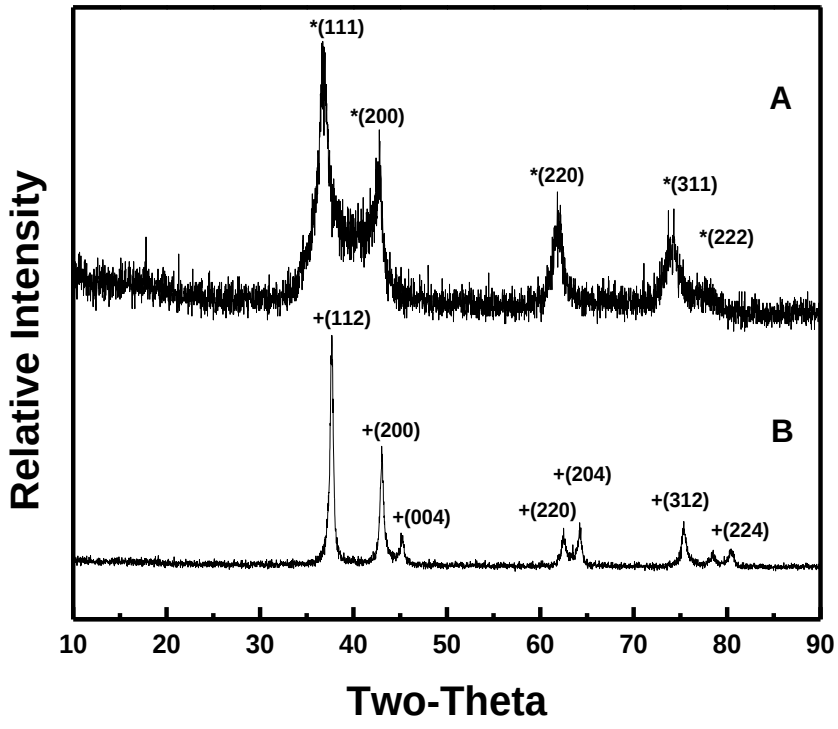

Figure 2.1 XRD patterns showing the reaction products of $(NH_4)_2Mg(MoO_4)_2$ decomposed in **(A)** a 1:4 molar ratio of CO-H_2 at 675 °C for ~1.0 hours and **(B)** a 4:1 molar ratio of N_2-H_2 at 750 °C for ~ 1.5 hours. *All peaks are normalized to the α-$MoC_{(1-x)}$ (111) reflection in (A). Reflections of specific phases are denoted as follows: β-$MoN_{(1-x)}$ "+", α-$MoC_{(1-x)}$ "*". The sample in (A) was not etched by HCl.*

SEM images in Figure-2.2 shows a similar morphology as the materials obtained by the method in Chapter 1, with average particle sizes on the order of ~30 nm. The surface area of α-$MoC_{(1-x)}$ prepared by this method was measured by BET analysis to be ~32 m^2/g. This result is consistent with the observed particle size.

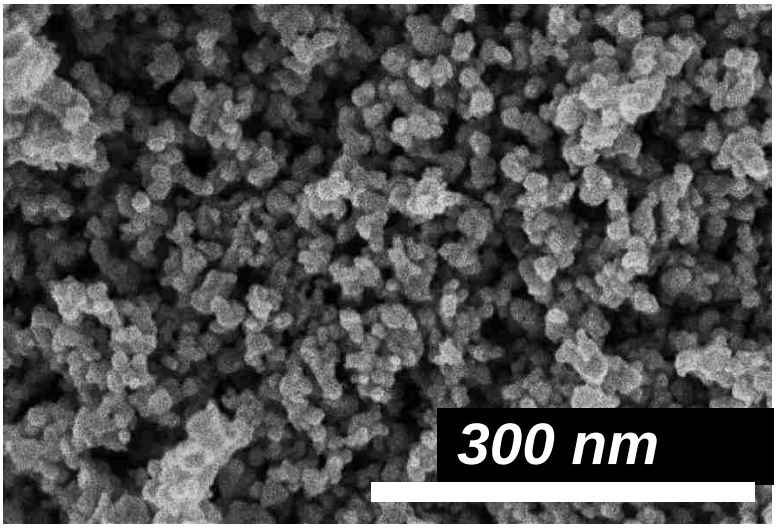

Figure 2. 2 SEM image of α-$MoC_{(1-x)}$ prepared the reaction $(NH_4)_2Mg(MoO_4)_2$ in a 1:4 molar flow of CO-H_2 at 675 °C for 1.5 hours. MgO was etched by HCl.

2.3.2 *In Situ* Synthesis of $PtMo_z$/α-$MoC_{(1-x)}$

For the *in situ* synthesis of $PtMo_z$/α-$MoC_{(1-x)}$, $H_2(PtCl_6)$ and $(NH_4)_2Mg(MoO_4)_2$ were found to form an amorphous white solid when an aqueous solution of the two compounds were precipitated using an excess of $NH_4(OH)$. This amorphous compound is likely a co-precipitated product of $(NH_4)_2Mg(MoO_4)_2$ and $(NH_4)_2(PtCl_6)$, although the exact nature of this compound remains undetermined. When heat treated under the carbiding conditions described previously, this amorphous compound was found to decompose to a platinum containing α-$MoC_{(1-x)}$ composite material. There was no metallic Pt or $PtMo_z$ phases observed in XRD, shown in Figure-2.3. The theoretical platinum loading of 8 wt% was consistent with X-ray fluorescence measurements

(XRF) showing an actual loading of ~7.5 wt% Pt. These results suggest the presence of highly dispersed $PtMo_z$ phases.

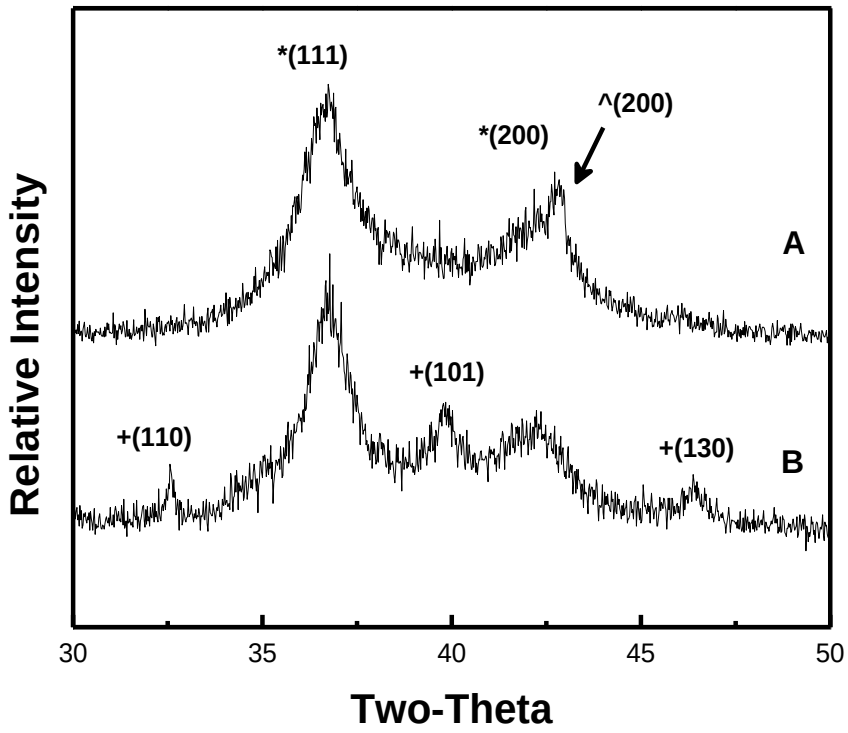

Figure 2.3 XRD patterns showing the reaction products of **(A)** the precipitated product of $(NH_4)_2Mg(MoO_4)_2$ and $Mg(MoO_4)$ in an excess of $NH_4(OH)$ and **(B)** $(NH_4)_2Mg(MoO_4)_2$ and $Mg(MoO_4)$ crystallized from solution without precipitation in $NH_4(OH)$. (*MgO in the catalyst shown in (A) was not etched by HCl*)

Cyclic voltammetry in deaerated 0.1M $HClO_4$, however, showed no evidence of platinum oxidation/reduction, H_2 underpotential deposition (UPD), or H_2 adsorption/stripping (HAD) peaks suggesting the absence of catalytically active Pt surface species. RDE experiments in O_2 saturated 0.1M $HClO_4$ revealed no cathodic activity and confirmed this material to be catalytically inert for ORR.

2.3.3 Catalyst activation by CO Surface Treatment

Since the as produced catalyst was found to be inactive for ORR, an activation

procedure was developed involving a surface treatment in pure CO directly following the thermal synthesis of the composite material in syngas (1:4 ratio of CO-H_2). The use of CO as an adsorbate which can induce the segregation of certain species within an alloy have been reported, typically applied to platinum by electrochemical adsorption of CO in saturated electrolyte [41]. Although electrochemical adsorption of CO was attempted to activate Pt phases within these materials, this was only found to have limited effect. A thermal method was attempted in which samples were cooled from the synthesis temperature of 675 °C to a slightly lower temperature, ranging from 450 °C to 650 °C, where the CO surface treatment would be administered. Once the new target temperature was reached the feed was switched to a pure CO atmosphere. Samples were then treated for an additional 2 hours under these conditions. XRD patterns for the catalysts prepared after the surface treatment, Figure-2.4, show no evidence of Pt or $PtMo_z$ phases found in the region between 36 ° - 40 ° in two-theta, the region where the (111) reflections of these species would be observed. A subtle decrease in the peak width at half maximum for the (111) reflection of α-$MoC_{(1-x)}$ was found with increasing surface treatment temperature, being most pronounced for samples treated at 650 °C. This result is attributed grain coarsening due to high temperature sintering of the α-$MoC_{(1-x)}$ domains. Crystallite domain size (XS) was calculated using whole pattern refinement in MDI JADE analytical software, where the domains were calculated to be approximately 1.5 nm larger for the sample treated in CO at 650 °C compared to the sample treated at 450 °C.

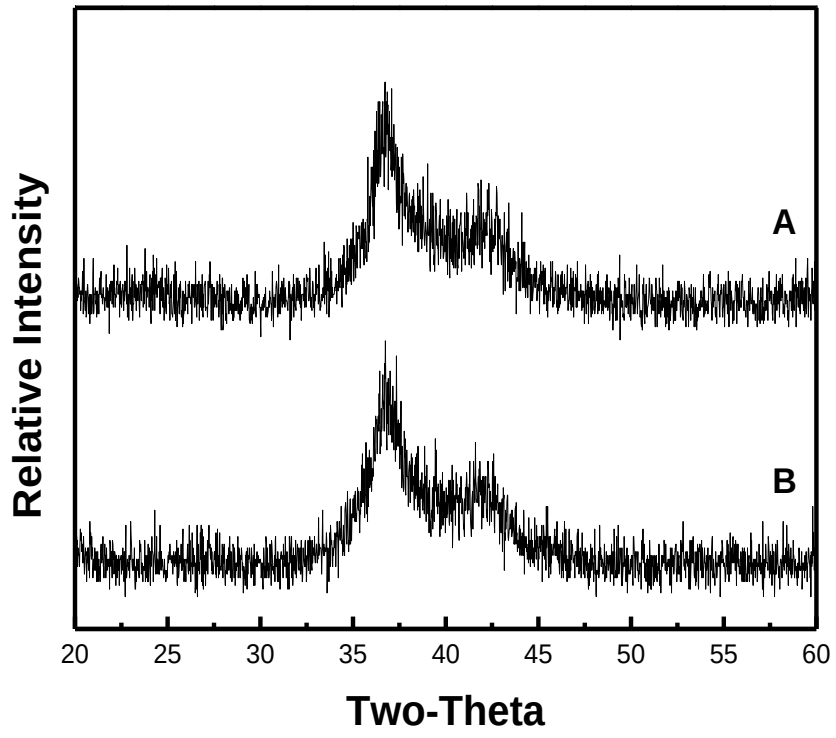

Figure 2.4 XRD patterns showing 8 wt% Pt/α-$MoC_{(1-x)}$ prepared from the precipitate formed by the reaction of $H_2(PtCl_6)$ and $(NH_4)_2Mg(MoO_4)_2$ in $NH_4(OH)$. Samples were treated in a 1:4 molar ratio of CO-H_2 at 675 °C for 1 hour followed by a surface treatment in pure CO for 2 hours at **(A)** 650 °C, XS = ~6.8 nm and **(B)** 450 °C, XS = ~5.3 nm.

2.3.4 Electrochemical Characterization

Following the CO surface treatment, these materials were found to possess characteristic Pt features in cyclic voltammetry, including: H_2 UPD, H_2 adsorption, and H_2 stripping when cycled in N_2 saturated perchloric acid, Figure-3. Using the H_2 adsorption peak from CV data, the electrochemical surface area was calculated from the following equation:

$$ECSA = \frac{Q_{Pt}}{210\frac{\mu C}{cm^2_{Pt}} \times L} \tag{10}$$

Here, Q_{pt} is the charge density calculated by the integration of the HAD peak (C/cm^2), 210 is the charge required to reduce a monolayer of protons on the electrode, and L is the catalyst loading on the electrode (g_{pt}/cm^2).

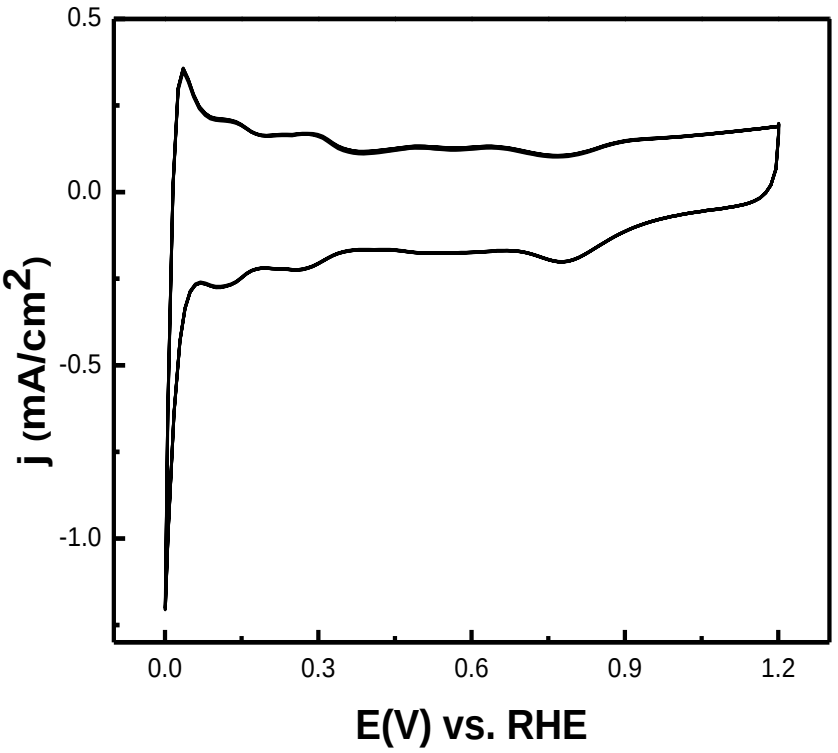

Figure 2.5 Cyclic voltammogram at 100 mV/s of 8 wt% Pt/α-$MoC_{(1-x)}$ in deaerated 0.1M $HClO_4$ after CO surface treatment at 650 °C for 2 hours.

From this, it was found that samples treated in CO at 650 °C had an ECSA of ~36 m^2/g_{pt}, indicating significant development of catalytic surface area as a direct result of the surface treatment in CO. ORR activity was measured using RDE experiments in a half cell configuration with O_2 saturated 0.1M $HClO_4$ at 100, 225, 400, 625, and 900 RPM at a scan rate of 5 mV/s (Figure-2.4). The half wave potential, $E_{1/2}$, was calculated as the potential corresponding to 50 % of the diffusion limited current, found to be 0.78 V vs RHE. The corresponding onset potential was found to be 1.01 V

vs RHE, an approximate overpotential of 50-100 mV for ORR when compared to values typically reported for that of platinum supported on carbon black [42-45].

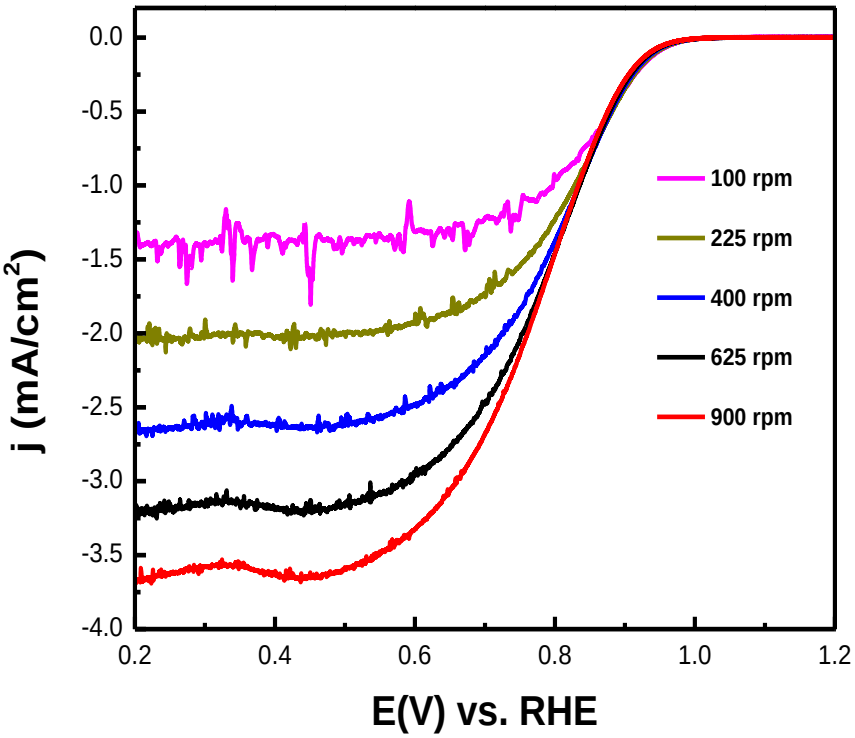

Figure 2.6 RDE measurements at 5 mV/s in O_2 saturated 0.1M $HClO_4$ for Pt/α-$MoC_{(1-x)}$ following CO surface treatment at 650 °C for 2 hours.

The Levich equation was used to estimate the number of electrons in the reaction transfer mechanism, ~3.8 e^-, calculated from the mass transfer limited current density, j_L:

$$n = \frac{j_L \upsilon^{(1/6)}}{0.62FD^{(2/3)}\omega^{(1/2)}C_{CO_2}} \tag{11}$$

where j_{Lev} is the limited current density (A/cm^2), ν is the kinematic viscosity of the electrolyte solution (St), F is the Faraday constant (C/mol), D is the diffusion coefficient for O_2 in the electrolyte (cm^2/s) ω is the angular frequency of the electrode (rad/s), and C is the concentration of O_2 in the electrolyte (mol/cm^3). Additionally, the platinum mass

activity, i_m, was calculated from RDE data using the following equation corrected for the mass transfer limited current density:

$$i_m = \frac{j_L \times j}{\left(j_L - j\right) \times L} \tag{12}$$

The result is shown in Figure-2.6 for data collected at 900 RPM, were the mass activity evaluated at 0.9 V vs RHE was found to be ~ 137 A/g_{pt}. Again, this result is consistent with values of mass activity for Pt/C_{black} commonly reported [39-40].

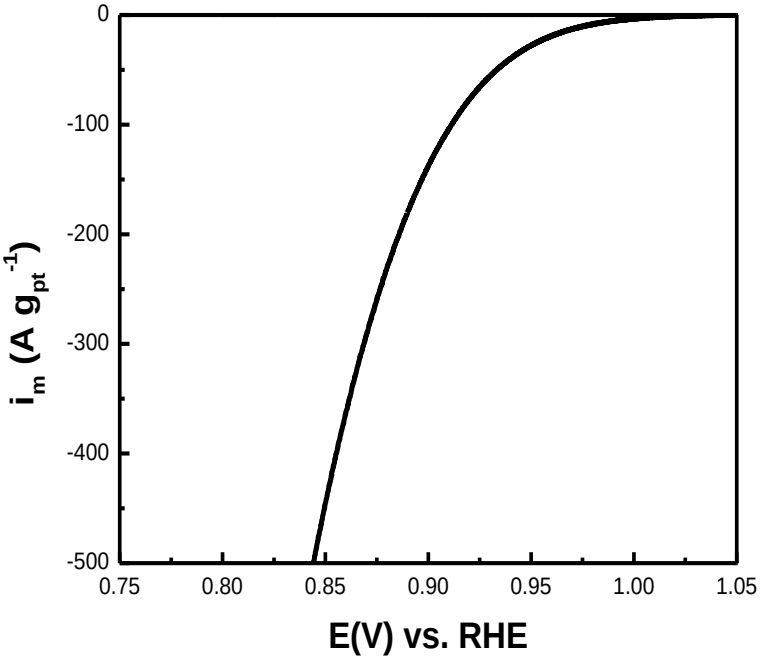

Figure 2.7 Platinum mass activity calculated from RDE data at 900 RPM and a scan rate of 5 mV/s in O_2 saturated 0.1M $HClO_4$ for Pt/α-$MoC_{(1-x)}$ following CO surface treatment at 650 °C for 2 hours.

2.3.5 XPS Analysis

Although bulk composition of the catalyst was seen to be unaffected by the CO surface treatment, substantial development in catalytic activity and surface area confirms either morphological or chemical changes in the surface environment of the α-$MoC_{(1-x)}$

supported $PtMo_z$ composite phases, however subtle these changes may be. To investigate the effect of surface treatment temperature, four catalysts were prepared and characterized using XPS surface analysis where the surface treatment temperatures were incremented as follows: 450 °C, 550 °C, 600 °C, and 650 °C. All samples were treated for the same duration, 2 hours, in pure CO.

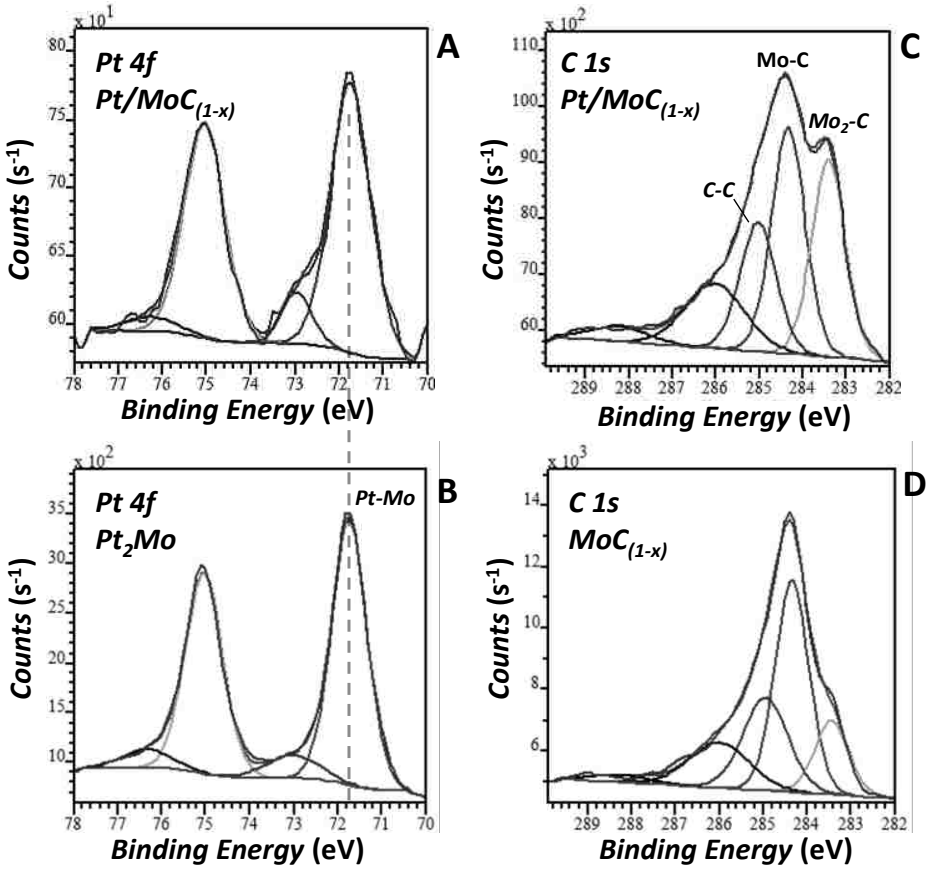

Figure 2. 8 XPS spectra showing the binding energies of the Pt 4f orbital for **(A)** 8 wt% Pt/α-$MoC_{(1-x)}$ CO treated at 650 °C and **(B)** Pt_2Mo, and for the C 1s orbital for **(C)** 8 wt% Pt/α-$MoC_{(1-x)}$ CO treated at 450 °C, and **(D)** 8 wt% Pt/α-$MoC_{(1-x)}$ CO treated at 650 °C

Platinum 4f binding energies were compared to a Pt_2Mo reference prepared by the high temperature reduction of MoO_2 and $H_2(PtCl_6)$, shown in Figure-2.8A and 2.8B respectively. The platinum environment for the 8 wt% Pt/α-$MoC_{(1-x)}$ catalysts CO treated

at temperatures from 450 °C to 650 °C were found to be similar to the Pt environment of the Pt_2Mo reference, with a dominant binding energy of 71.8 eV. The absence of a Pt-Pt binding energy, typically found near 71.2 eV for bulk Pt materials, suggest the presence of $PtMo_z$ intermetallic and solid solution phases by direct comparison of the Pt_2Mo reference. The dominant Pt 4f binding energy and corresponding distributions were found to remain relatively constant with increased CO treatment temperature. However, it is possible that the only observed Pt 4f binding energy, 71.8 eV, is a result of platinum oxide, Pt^{2+}, where a monolayer of platinum oxide is responsible for the observed binding energy. This would suggest that the similarity in the Pt 4f binding energies of the 8 wt% Pt/α-$MoC_{(1-x)}$ catalyst and the Pt_2Mo reference is coincidental and not evidence that the two materials are of similar or identical composition [46].

Analysis of the C 1s spectra, Figure-2.8C and 2.8D, revealed a trend correlating the C-Mo ratio as a function of increasing surface treatment temperature. Figure-2.9 plots the ratio of MoC to Mo_2C calculated from the C 1s spectra, deconvoluted into the XPS spectra for MoC, Mo_2C, and C-C, as a function of surface treatment temperature.

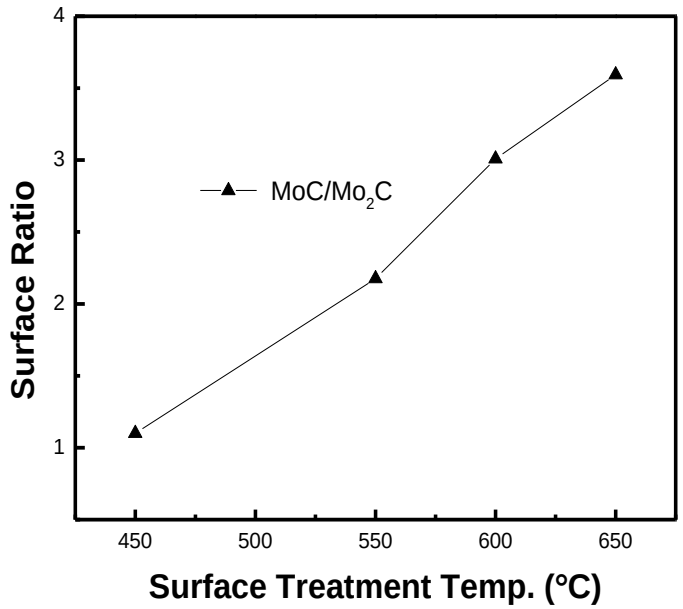

Figure 2. 9 Ratio of MoC to Mo_2C on the surface of 8 wt% Pt/$MoC_{(1-x)}$ as a function of CO surface treatment temperature calculated from XPS spectra of carbon 1s binding energies.

It was found that increasing the CO surface treatment temperature results in a shift to a more carbon rich phase of α-$MoC_{(1-x)}$ on the catalyst surface. An initial ratio of MoC:Mo_2C of 1:1 was significantly increased to ~ 3.5:1 following the CO treatment at 650 °C. Although this result may be expected for an additional heat treatment of molybdenum carbide in a carbonaceous atmosphere, it is unclear if this result has any significance in the dramatic development of surface activity following the CO treatment.

2.3.6 TEM Analysis

TEM analysis, shown in Figure-2.10, reveals crystallite domains for α-$MoC_{(1-x)}$, as well as various platinum phases of various domain size, on the approximate order of 5-10 nm. The observed polycrystalline particle structure is consistent with XRD observations of particle domain size. To confirm the existence of specific $PtMo_z$ phases,

lattice fringes were indexed using spot diffraction patterns created by Fourier Form Transform using GATAN Digital Micrograph software. Lattice d-spacings were indexed in the region of 2.22 Å to 2.35 Å due to the increased resolution between (111) reflections of α-Pt phases, the (210) reflection of cP α-$PtMo_z$ phases, (111) reflections of the cF α-$PtMo_z$, and the (111) reflection of the tetragonal $PtMo_z$ phase found in this region. Additionally, this is the region in which the 100% lines of these phases, again typically the (111) reflections, would be observed in XRD.

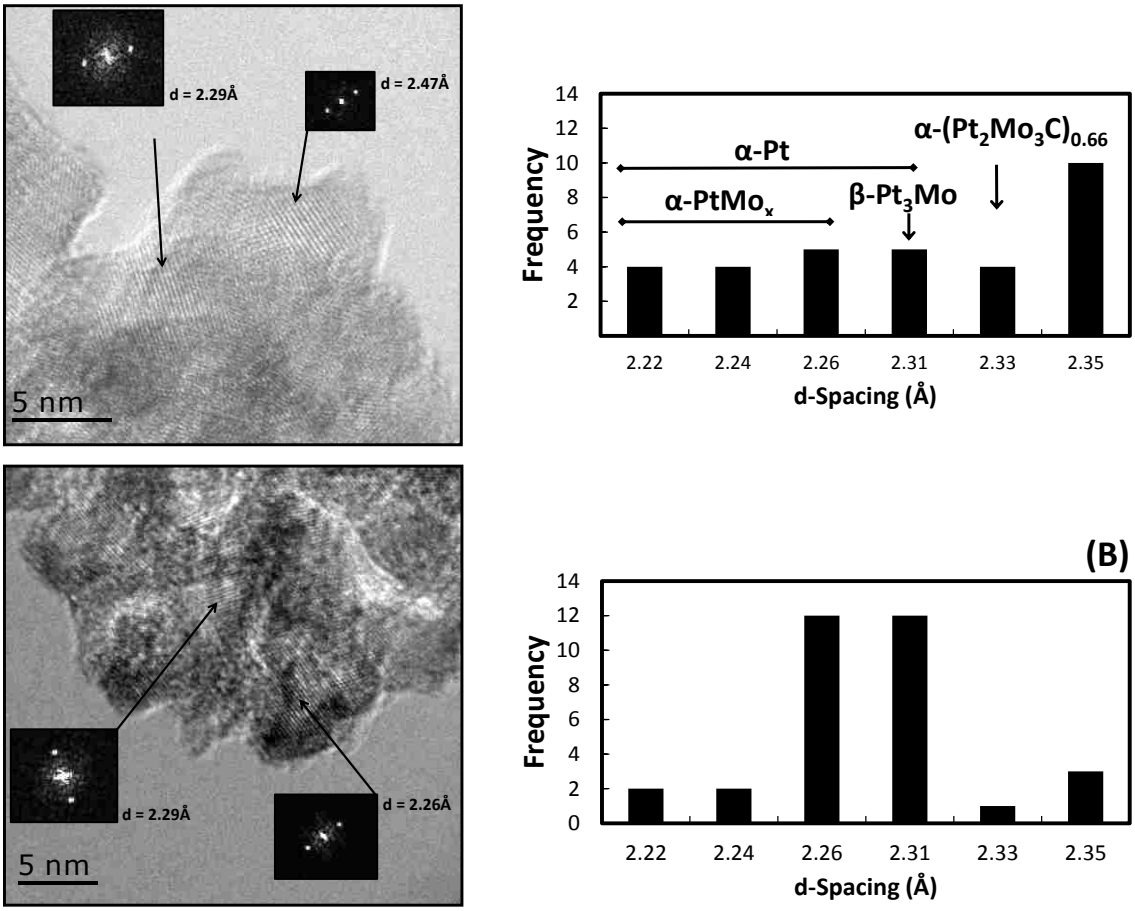

Figure 2.10 TEM images and corresponding histograms showing the distribution of Pt and $PtMo_z$ phases for **(A)** 8 wt% Pt/α-$MoC_{(1-x)}$ prior to a CO surface treatment 650 °C for 2 hours and **(B)** 8 wt% Pt/α-$MoC_{(1-x)}$ after a CO surface treatment at 650 °C for 2 hours.

The results show that prior to the CO surface treatment there was a broad distribution of Pt and/or $PtMo_z$ phases observed, with a majority concentrated in the region of 2.26 Å and 2.31 Å. Identification of specific phases was not possible due to a large overlap in the d-spacing of various Pt and $PtMo_z$ phases in this region, a result of the isostructural nature of these materials. Following the CO surface treatment, the distribution of $PtMo_z$ phases was found to be spread more broadly throughout the entire region. Although there is no clear evidence of a shift from one phase in particular to another, it is clear that the CO surface treatment is inducing a redistribution of the $PtMo_z$ phases. It is hypothesized that this redistribution results in the exposure of certain Pt or $PtMo_z$ facets on the surface of the material. This result is consistent with the development of catalytic activity confirmed by CV measurements, where catalytic activity is strictly a surface phenomenon.

Evidence of a ternary Pt-Mo-C phase can also be found in the region of 2.33 Å, corresponding to a lattice parameter too large to be associated with any cubic Pt or $PtMo_z$ compound published in various crystal structure databases, as shown in Figure-2.10B. The preparation of this particular ternary phase is consistent with the direct high temperature reaction of the constituent species [47]. This phase was found in slightly higher concentrations following the CO surface treatment, yet it is unclear if this phase contributes to the developed catalytic activity resulting from the surface treatment.

The most significant observation found in the materials following the CO surface treatment is the formation of a phase with the corresponding d-spacing of 2.35 Å. This phase is attributed to the (103) reflection of hexagonal β-$MoC_{(1-x)}$, a transition within the

molybdenum carbide species which may be related to the segregation of carbide and $PtMo_z$ phases. This determination is supported by XRD analysis which reveals no bulk shift from cubic to hexagonal β-$MoC_{(1-x)}$, which when compared to TEM analysis suggests an extent of phase transition within the carbide phase on the same order as the transitions within the $PtMo_z$ phases.

2.4 Conclusion

An *in situ* method of dispersing $PtMo_z$ on α-$MoC_{(1-x)}$ was successfully developed which involves the integration of Pt and Mo precursors, allowing for the simultaneous synthesis of catalyst and catalyst support species without significant sintering and agglomeration of the Pt phases. A CO surface treatment was successfully used to tune the surface properties/composition of the material transforming it from an inert to an active catalyst for ORR. The development of ECSA following the surface treatment, ~ 36 m^2/g_{pt}, and Pt mass activity of ~ 137 A/g_{pt}, demonstrates the success of this method in creating an active catalyst for ORR. The lack of crystalline $PtMo_z$ phases observed in XRD as well as TEM analysis suggests a particles size of the $PtMo_z$ phases estimated to be on the order of ~ 5 nm, further demonstrating the success of the method for dispersing $PtMo_z$ nano-particles on the surface of the the α-$MoC_{(1-x)}$ support. However, kinetic measurements for ORR, $E_{1/2}$ of ~ 0.78 V vs. RHE with an onset potential of ~ 1.01 V vs. RHE, show this catalysts suffers from an overpotential for ORR approximately 50-100 mV greater than that of P/C_{black}. Additionally, preliminary durability studies (see Appendix-B) suggest this catalyst does not possess any improvement in durability compared to Pt/C_{black}. Although catalyst degradation is observed, the mode of degradation

remains unidentified (dissolution of the α-$MoC_{(1-x)}$ support, dissolution of $PtMo_z$, or a combination of the two processes).

Thesis Conclusion

Pertaining to the objectives identified within the scope of this project, a method for preparing high surface area α-$MoC_{(1-x)}$, and β - $MoN_{(1-x)}$, without the requirement of temperature programmed reduction (TPR) has been achieved. $Mg(MoO_4)$ and $Zn(MoO_4)$ have been demonstrated to decompose, through a preferred non-oxide (MoO_2) reaction pathway, to high surface area α-$MoC_{(1-x)}$ (35 m^2/g and 45 m^2/g respectively) using syngas as a carbon source. The capability of producing β-$MoN_{(1-x)}$ without TPR and in an NH_3 free synthesis (using forming gas as a N_2 source) has also been demonstrated.

This result led to the development of a more effective precursor, $(NH_4)_2Mg(MoO_4)_2$, which was found to decompose to α-$MoC_{(1-x)}$ in syngas at a rate two times greater, while at lower temperature, than $Mg(MoO_4)$. β - $MoN_{(1-x)}$ was also found to form more readily when this ammonium molybdate derived precursor was used.

A facile method of producing highly dispersed Pt phases, active for oxygen reduction reaction, on α-$MoC_{(1-x)}$ has also been accomplished. The integration of Pt and Mo precursors using a chemical precipitation method made possible the simultaneous synthesis of α-$MoC_{(1-x)}$, the support species, and $PtMo_z$, the catalyst species. The simultaneous synthesis of the catalyst and support address the logistical difficulties of dispersing Pt on α-$MoC_{(1-x)}$ without the exposure of α-$MoC_{(1-x)}$ to air.

Although the $PtMo_z$ composite catalyst supported on α-$MoC_{(1-x)}$ was found to be active for ORR, as characterized by cyclic voltammetry, the durability of this catalyst does not appear to offer any improvements to the limited durability of Pt/C_{black}.

References

1. Oh, H. S.; Lee, J. H.; Kim, H., Electrochemical carbon corrosion in high temperature proton exchange membrane fuel cells. *Int. J. Hydrog. Energy* 2012, *37* (14), 10844-10849.

2. Shao, Y. Y.; Yin, G. P.; Gao, Y. Z., Understanding and approaches for the durability issues of Pt-based catalysts for PEM fuel cell. *J. Power Sources* 2007, *171* (2), 558-566.

3. Blackmore, K. J.; Elbaz, L.; Bauer, E.; Brosha, E. L.; More, K.; McCleskey, T. M.; Burrell, A. K., High Surface Area Molybdenum Nitride Support for Fuel Cell Electrodes. *J. Electrochem. Soc.* 2011, *158* (10), B1255-B1259.

4. Hugosson, H. W.; Jansson, U.; Johansson, B.; Eriksson, O., Phase stability diagrams of transition metal carbides, a theoretical study. *Chem. Phys. Lett.* 2001, *333* (6), 444-450.

5. Oshikawa, K.; Nagai, M.; Omi, S., Characterization of molybdenum carbides for methane reforming by TPR, XRD, and XPS. *J. Phys. Chem. B* 2001, *105* (38), 9124-9131.

6. Kojima, R.; Aika, K., Molybdenum nitride and carbide catalysts for ammonia synthesis. *Appl. Catal. A-Gen.* 2001, *219* (1-2), 141-147.

7. Wu, Q. X.; Christensen, J. M.; Chiarello, G. L.; Duchstein, L. D. L.; Wagner, J. B.; Temel, B.; Grunwaldt, J. D.; Jensen, A. D., Supported molybdenum carbide for higher alcohol synthesis from syngas. *Catal. Today* 2013, *215*, 162-168.

8. Hynaux, A.; Sayag, C.; Suppan, S.; Trawczynski, J.; Lewandowski, M.; Szymanska-Kolasa, A.; Djega-Mariadassou, G., Kinetic study of the hydrodesulfurization of dibenzothiophene over molybdenum carbides supported on functionalized carbon black composite - Influence of indole. *Appl. Catal. B-Environ.* 2007, *72* (1-2), 62-70.

9. Ramanathan, S.; Yu, C. C.; Oyama, S. T., New catalysts for hydroprocessing: Bimetallic oxynitrides II. Reactivity studies. *J. Catal.* 1998, *173* (1), 10-16.

10. Vrubel, H.; Hu, X. L., Molybdenum Boride and Carbide Catalyze Hydrogen Evolution in both Acidic and Basic Solutions. *Angew. Chem.-Int. Edit.* 2012, *51* (51), 12703-12706.

11. Volpe, L.; Boudart, M., Compounds of Molybdenum and Tungsten with High Specific Surface-Area-.2. Nitrides. *J. Solid State Chem.* 1985, *59* (3), 332-347.

12. Volpe, L.; Boudart, M., Compounds of Molybdenum and Tungsten with High Specific Surface-Area-.2. Carbides. *J. Solid State Chem.* 1985, *59* (3), 348-356.

13. Bouchy, C.; Hamid, S.; Derouane, E. G., A new route to the metastable FCC molybdenum carbide alpha-MoC1-x. *Chem. Commun.* 2000, (2), 125-126.

14. Zhu, Q. L.; Chen, Q. G.; Yang, X. B.; Ke, D. X., A new method for the synthesis of molybdenum carbide. *Mater. Lett.* 2007, *61* (29), 5173-5174.

15. Patel, M.; Subrahmanyam, J., Synthesis of nanocrystalline molybdenum carbide (Mo2C) by solution route. *Mater. Res. Bull.* 2008, *43* (8-9), 2036-2041.

16. Hanif, A.; Xiao, T. C.; York, A. P. E.; Sloan, J.; Green, M. L. H., Study on the structure and formation mechanism of molybdenum carbides. *Chem. Mat.* 2002, *14* (3), 1009-1015.

17. Weimer, A. W., Carbide, Nitride, and Boride Materials Synthesis and Processing. Chapman & Hall: London, 1997; p 79-80.

18. Wise, R. S.; Markel, E. J., Synthesis of high-Surface-Area Molybdenum Nitride in Mixtures of Nitrogen and Hydrogen. *J. Catal.* 1994, *145* (2), 344-355.

19. Robson, M. H.; Serov, A.; Artyushkova, K.; Atanassov, P., A mechanistic study of 4-aminoantipyrine and iron derived non-platinum group metal catalyst on the oxygen reduction reaction. *Electrochim. Acta* 2013, *90*, 656-665.

20. Brocato, S.; Serov, A.; Atanassov, P., pH dependence of catalytic activity for ORR of the non-PGM catalyst derived from heat-treated Fe-phenanthroline. *Electrochim. Acta* 2013, *87*, 361-365.

21. Serov, A.; Robson, M. H.; Artyushkova, K.; Atanassov, P., Templated non-PGM cathode catalysts derived from iron and poly(ethyleneimine) precursors. *Appl. Catal. B-Environ.* 2012, *127*, 300-306.

22. Serov, A.; Robson, M. H.; Smolnik, M.; Atanassov, P., Templated bi-metallic non-PGM catalysts for oxygen reduction. *Electrochim. Acta* 2012, *80*, 213-218.

23. Serov, A.; Martinez, U.; Falase, A.; Atanassov, P., Highly active Pd-Cu catalysts for electrooxidation of 2-propanol. *Electrochem. Commun.* 2012, *22*, 193-196.

24. Falase, A.; Main, M.; Garcia, K.; Serov, A.; Lau, C.; Atanassov, P., Electrooxidation of ethylene glycol and glycerol by platinum-based binary and ternary nano-structured catalysts. *Electrochim. Acta* 2012, *66*, 295-301.

25. Weirich, F. A. A Study of the Reduction of Zinc Oxide by Hydrogen and Methane School of Mines and Metallurgy of the University of Missouri, Rolla, Mo, 1926.

26. Belgued, M.; Pareja, P.; Amariglio, A.; Amariglio, H., Conversion of Methane Into Higher Hydrocarbons on Platinum. *Nature* 1991, *352* (6338), 789-790.

27. Davis, R. J.; Derouane, E. G., A Nonporous Supported-Platinum Catalyst For Aromization Of N-Hexane. *Nature* 1991, *349* (6307), 313-315.

28. Liang, C. C.; Juliard, A. L., Reduction of Oxygen at Platinum Electrode. *Nature* 1965, *207* (4997), 629-&.

29. Tian, N.; Zhou, Z. Y.; Sun, S. G.; Ding, Y.; Wang, Z. L., Synthesis of tetrahexahedral platinum nanocrystals with high-index facets and high electro-oxidation activity. *Science* 2007, *316* (5825), 732-735.

30. Tupy, S. A.; Chen, J. G. G.; Vlachos, D. G., Comparison of Ethylene Glycol Steam Reforming Over Pt and NiPt Catalysts on Various Supports. *Top. Catal.* 2013, *56* (18-20), 1644-1650.

31. Obradovic, A.; Likozar, B.; Levec, J., Catalytic surface development of novel nickel plate catalyst with combined thermally annealed platinum and alumina coatings for steam methane reforming. *Int. J. Hydrog. Energy* 2013, *38* (3), 1419-1429.

32. Serov, A.; Martinez, U.; Atanassov, P., Novel Pd-In catalysts for alcohols electrooxidation in alkaline media. *Electrochem. Commun.* 2013, *34*, 185-188.

33. Serov, A.; Robson, M. H.; Smolnik, M.; Atanassov, P., Tri-metallic transition metal–nitrogen–carbon catalysts derived by sacrificial support method synthesis. *Electrochim. Acta* 2013, *109* (0), 433-439.

34. Robson, M. H.; Serov, A.; Artyushkova, K.; Atanassov, P., A mechanistic study of 4-aminoantipyrine and iron derived non-platinum group metal catalyst on the oxygen reduction reaction. *Electrochim. Acta* 2013, *90*, 656-665.

35. Bashyam, R.; Zelenay, P., A class of non-precious metal composite catalysts for fuel cells. *Nature* 2006, *443* (7107), 63-66.

36. Wu, G.; More, K. L.; Johnston, C. M.; Zelenay, P., High-Performance Electrocatalysts for Oxygen Reduction Derived from Polyaniline, Iron, and Cobalt. *Science* 2011, *332* (6028), 443-447.

37. Lefevre, M.; Proietti, E.; Jaouen, F.; Dodelet, J. P., Iron-Based Catalysts with Improved Oxygen Reduction Activity in Polymer Electrolyte Fuel Cells. *Science* 2009, *324* (5923), 71-74.

38. Weidman, M. C.; Esposito, D. V.; Hsu, Y. C.; Chen, J. G., Comparison of electrochemical stability of transition metal carbides (WC, W2C, MO2C) over a wide pH range. *J. Power Sources* 2012, *202*, 11-17.

39. Kriston, A.; Xie, T. Y.; Gamliel, D.; Ganesan, P.; Popov, B. N., Effect of ultra-low Pt loading on mass activity of polymer electrolyte membrane fuel cells. *J. Power Sources* 2013, *243*, 958-963.

40. Patel, S.; Jiang, J. C.; Liu, F. Q., Facile synthesis and characterization of highly dispersed platinum nanoparticles for fuel cells. *Int. J. Hydrog. Energy* 2011, *36* (17), 11108-11115.

41. Andersson, K. J.; Calle-Vallejo, F.; Rossmeisl, J.; Chorkendorff, L., Adsorption-Driven Surface Segregation of the Less Reactive Alloy Component. *J. Am. Chem. Soc.* 2009, *131* (6), 2404-2407.

42. Wu, J. B.; Yang, H., Platinum-Based Oxygen Reduction Electrocatalysts. *Accounts Chem. Res.* 2013, *46* (8), 1848-1857.

43. Job, N.; Chatenet, M.; Berthon-Fabry, S.; Hermans, S.; Maillard, F., Efficient Pt/carbon electrocatalysts for proton exchange membrane fuel cells: Avoid chloride-based Pt salts! *J. Power Sources* 2013, *240* (0), 294-305.

44. Santos, L. G. R. A.; Freitas, K. S.; Ticianelli, E. A., Heat treatment effect of Pt–V/C and Pt/C on the kinetics of the oxygen reduction reaction in acid media. *Electrochim. Acta* 2009, *54* (22), 5246-5251.

45. Hayden, B. E.; Pletcher, D.; Suchsland, J. P.; Williams, L. J., The influence of support and particle size on the platinum catalysed oxygen reduction reaction. *Phys. Chem. Chem. Phys.* 2009, *11* (40), 9141-9148.

46. Porsgaard, S.; Merte, L. R.; Ono, L. K.; Behafarid, F.; Matos, J.; Helveg, S.; Salmeron, M.; Cuenya, B. R.; Besenbacher, F., Stability of Platinum Nanoparticles Supported on SiO2/Si(111): A High-Pressure X-ray Photoelectron Spectroscopy Study. *ACS Nano* 2012, *6* (12), 10743-10749.

47. Lawson, A. C., Superconductivity of the f.c.c. transition metals, and of their alloys and f.c.c. carbides. *Journal of the Less Common Metals* 1971, *23* (1), 103-106.

48. R. Ferro, M., R., The Mo-N (Molybdenum-Nitrogen) System. *Bulletin of Allow Phase Diagrams* 1980, *1* (2), 82-85.

49. FactSage STGE Solution Databse List of Systems and Phases. http://www.factsage.cn/fact/documentation/SGTE/SGTE_list.htm (accessed November 11, 2013).

Appendix-A

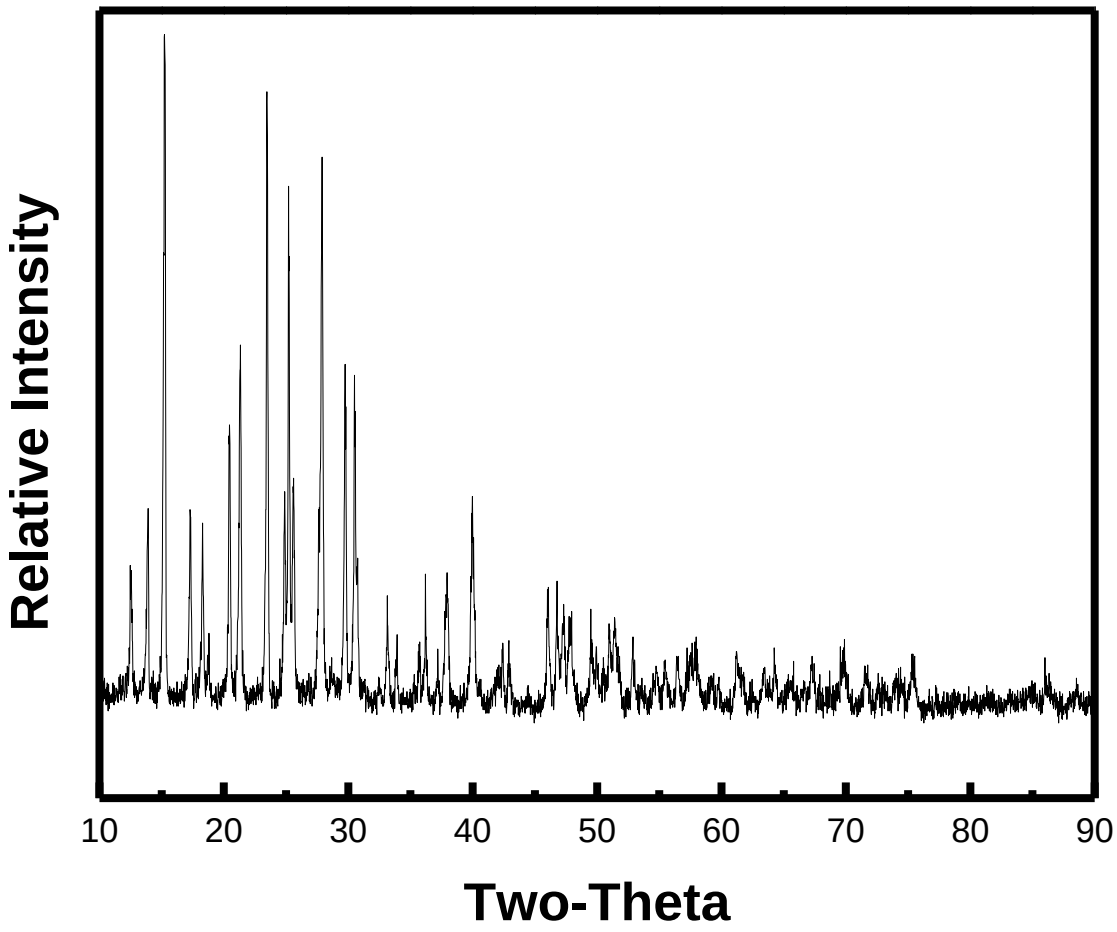

Appendix A. 1 XRD diffraction pattern for $(NH_4)_2Mg(MoO_4)_2$ obtained by the co-precipitation of $(NH_4)_2(MoO_4)$ with $Mg(MoO_4)$ in stoichiometric proportions. See Appendix A.2 for phase reflection data.

Intensity %	Angle, 2θ	d(Å)	(h k l)
24	12.5	7.062	(0 2 0)
26.4	13.9	6.3861	(1 0 0)
100	15.2	5.819	(1 1 0)
41.2	17.3	5.1285	(0 1 1)
36.4	18.3	4.8479	(-1 1 1)
51.5	20.4	4.3413	(0 2 1)
72.2	21.3	4.1671	(-1 2 1)
87.7	23.5	3.7895	(1 3 0)
40.3	24.9	3.5777	(0 3 1)
47.3	25.2	3.531	(0 4 0)
24	25.6	3.4809	(1 1 1)
32.1	25.6	3.4783	(-1 3 1)
24.8	27.6	3.2255	(-2 1 1)
85.3	27.8	3.2014	(1 2 1)
60.5	29.8	2.9994	(-2 2 1)
52.9	30.5	2.9289	(-1 0 2)
16.5	30.7	2.9095	(2 2 0)
15.7	38.0	2.3683	(2 4 0)
38.7	40.0	2.2543	(-1 4 2)
18.9	46.1	1.9688	(1 6 1)

Appendix A. 2 XRD diffraction data for $(NH_4)_2Mg(MoO_4)_2$. Phase PDF # [97-002-3001] taken from ICSD database.

Appendix-B

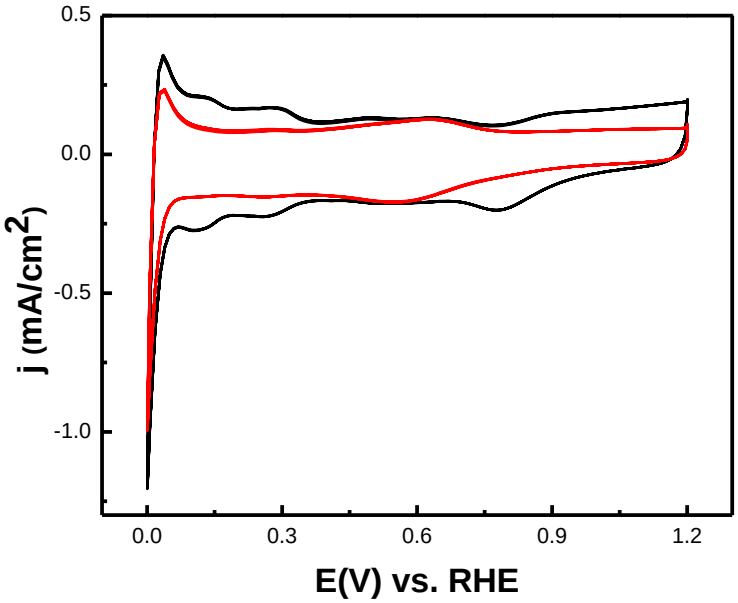

Appendix B. 1 CV of 8 wt% Pt/α-$MoC_{(1-x)}$ in N_2 saturated $HClO_4$ at 100 mV/s prior to durability study (Black, ECSA ~ 36 m^2/g) and after a durability study (Red, ECSA is below instrument resolution). Durability study was conducted in O_2 saturated $HClO_4$ using an RDE setup rotating at 900 RPM with a sweep rate of 100 mV/sec from 1.3 – 0.6 V vs. RHE. A total of 5000 cycles were used in the study.

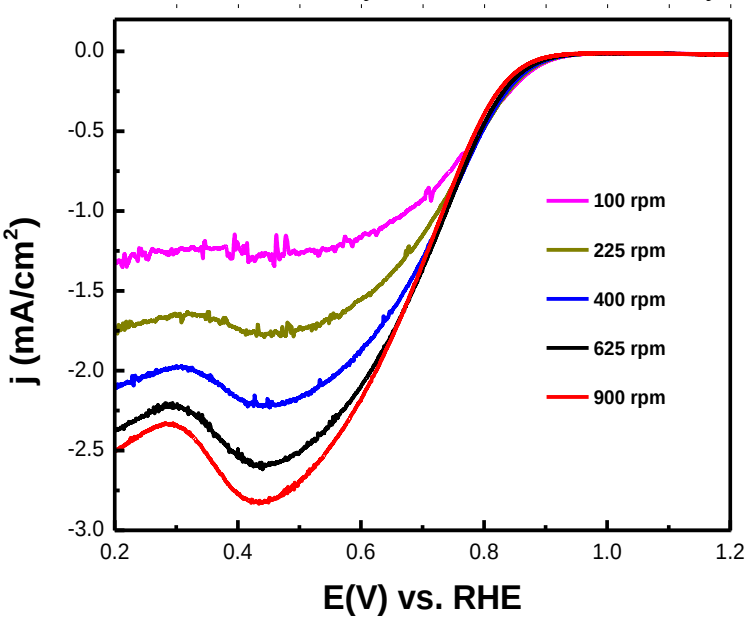

Appendix B. 2 CV of 8 wt% Pt/α-$MoC_{(1-x)}$ in O_2 saturated $HClO_4$ at 5 mV/s at various rotation speeds after the durability study, described by Appendix B.1.

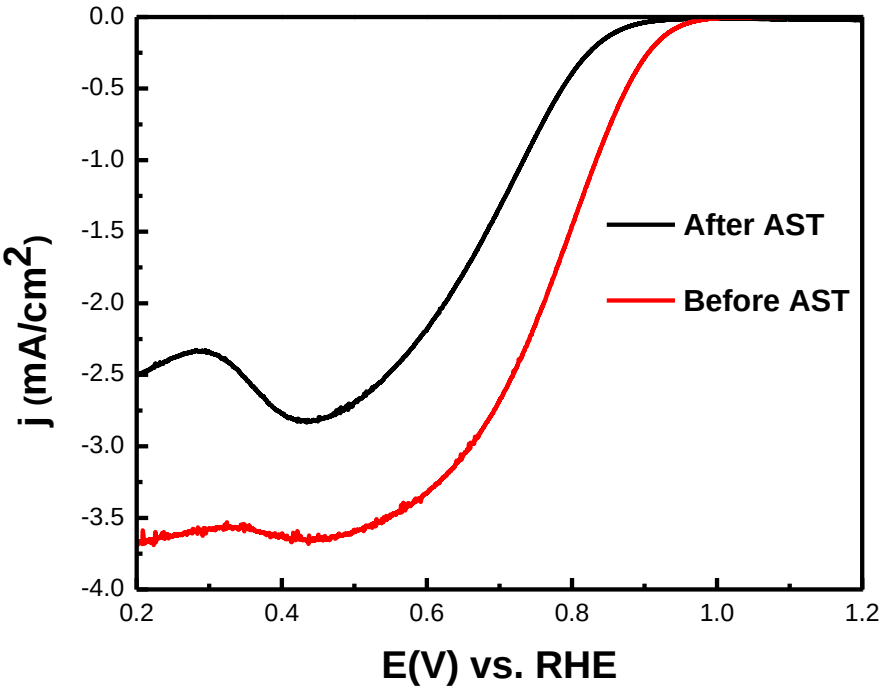

Appendix B. 3 Comparison of ORR activity before and after the durability study described by Appendix B.1.

Appendix-C

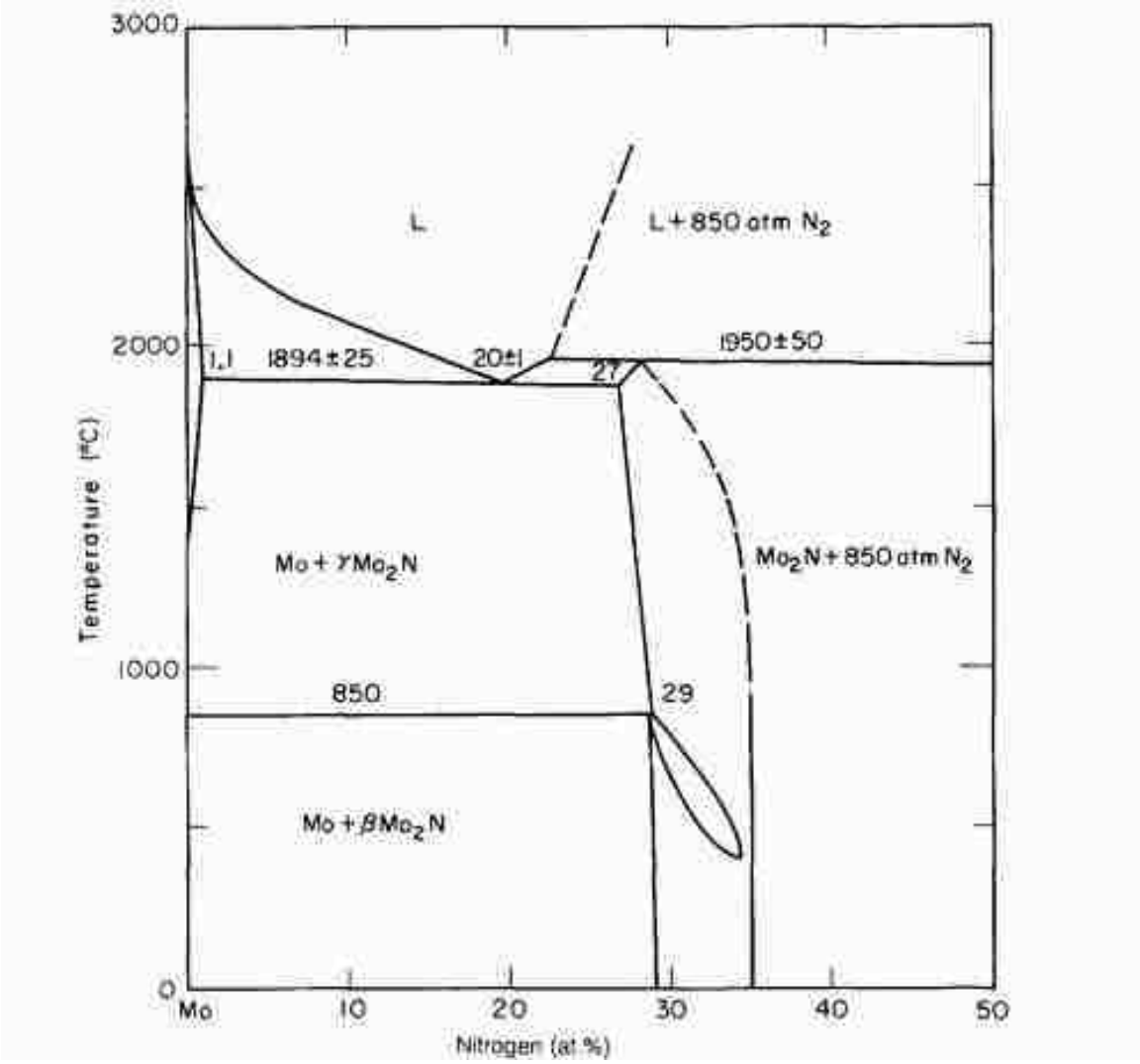

Appendix C.1 Mo-N phase *[48]*.

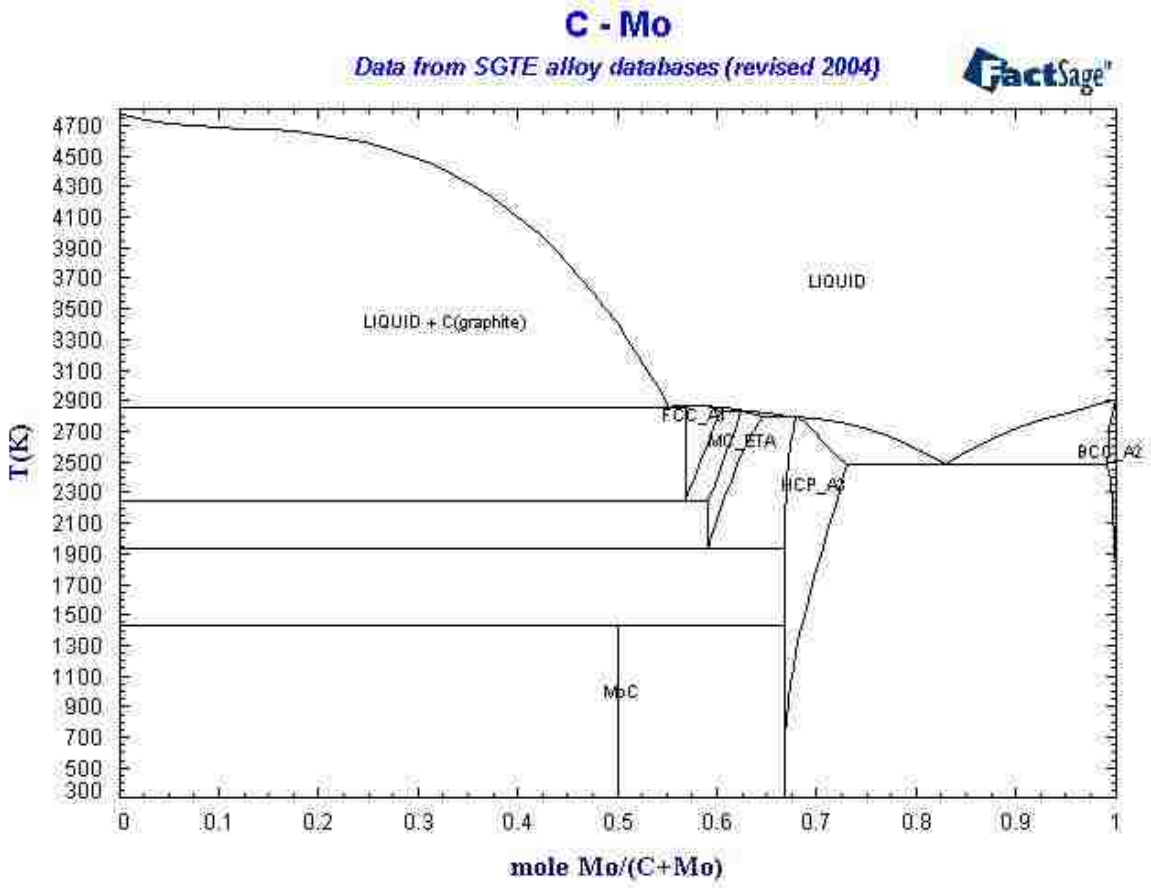

Appendix C.2 Mo-C phase diagram. *[49]*.